2008

Quasi-Static and Impact Characterization of Sandwich Structures with an Iso-Grid Stiffened Syntactic Foam Core

Venkata Sandeep Chakka
Louisiana State University and Agricultural and Mechanical College

QUASI-STATIC AND IMPACT CHARACTERIZATION OF SANDWICH STRUCTURES WITH AN ISO-GRID STIFFENED SYNTACTIC FOAM CORE

A Thesis

Submitted to the Graduate Faculty of the
Louisiana State University and
Agricultural and Mechanical College
in partial fulfillment of the
requirements for the degree of
Master of Science in Mechanical Engineering

in

The Department of Mechanical Engineering

by
Venkata Sandeep Chakka
B.E., Andhra University, Visakhapatnam, India, 2005
December 2008

ACKNOWLEDGEMENTS

I would like to extend my sincere gratitude to Dr. Guoqiang Li, my major Professor for the invaluable support and encouragement extended throughout my study. I would like to thank members of my graduate committee, Dr. Su-Seng Pang and Dr. Muhammad Wahab for offering heir precious time and to serve in the examination committee and evaluate my thesis. I would like to thank all the friends in my lab for providing technical and moral support. I wish to acknowledge the constant emotional support and guidance provided by my father, Mr. Suresh Gupta Chakka, my mother, Ms. Vijaya Lakshmi Chakka and my sister Sri Durga Chakka.

TABLE OF CONTENTS

LIST OF TABLES

LIST OF FIGURES

ABSTRACT

In this study, a novel hybrid sandwich structure with an integrated, iso-grid stiffened syntactic foam core was fabricated and evaluated by impact test and static test. Sandwich beams with different grid cell areas were prepared using a pin-guided dry weaving process. Low velocity impact test on different locations (rib, node, and bay) was conducted with varying hammer weight and impact velocities by an instrumented impact testing machine. Ultrasonic C-scan was utilized before and after impact to identify the damage induced by impact. Scanning Electron Microscopy observation was also implemented to visualize the impact damage at micro-length scale. Compressions after impact (CAI) tests per an anti-buckling test fixture were conducted to evaluate the residual strength and stiffness of the impact damaged sandwich plate specimens. In order to validate the experimental results, Finite Element Analysis was conducted on unimpacted specimens of different Groups. Parametric study was also conducted to study how different parameters affect the strength of the iso-grid stiffened sandwich structures. The test results show that the novel sandwich structure has a higher capacity to transfer impact energy elastically. It leads the sandwich plate towards quasi-static impact response. The propagation energy, the energy absorbed for damage creation and propagation, is reduced. The damage is more localized and confined to the bay directly under impact or adjacent bays. It is found that the bay area is one of the most important design parameters for the iso-grid pattern investigated. The residual strength and residual modulus of iso-grid structures is found to be higher than that of laminates. Impact damage on iso-grid structures is confined to a smaller area when compared to laminates.

CHAPTER 1. INTRODUCTION

Sandwich structures can be defined as the structures formed by combining two thin and stiff face sheets with a thick and relatively weak core [1]. Sandwich structures can be used in applications where high specific strength and bending stiffness are required. Sandwich structures have a wide variety of applications such as automobiles, commercial vessels, aviation sector etc. Skin acts as a stiffener and also protects the core from damage; core acts as a binder for the skin. In a sandwich structure, the skin carries all the bending loads and the core resists the in-plane loads and transverse shear loads [2]. Addition of the stiffener will enhance the dynamic properties of the structures. A metal sheet like aluminum, steel or glass fibers or carbon fibers reinforced polymer can be used for skin. The skin is attached to both sides of the core material using an adhesive. In the case of a syntactic foam core, the matrix acts as a binder. Another important characteristic of a sandwich structure is their high strength to weight ratio.

Properties of the core play an important role in the strength of the sandwich structures. Various types of cores are foam core, honey-comb core, truss core, which come under the category of web cores, 3-D integrated core [3], hollow integrated core [4], other types of web cores etc. Though foam core has a property to absorb energy, foam core is brittle. The problem with web core is that it doesn't bind properly with the skin which makes it prone to impact damage and skin buckling. In addition to the problems with web core, honey-comb core has a problem of buckling and has low strength to weight ratio [5-7]. Truss core has a problem of buckling due to impact [8]. Improper bonding of core and skin has a significant effect on the strength of sandwich structures.

Advanced grid stiffened composite structure is defined as a lattice of two, three, or four interlacing ribs. There are three types of basic grid structures which are bi-directional grid, tri-

directional grid and quadric-directional grid. Iso-grid is a type of grid stiffened structure which falls under tri-directional grid. The unit cell has the shape of an equilateral triangle. An iso-grid can be defined as a lattice of intersecting ribs forming an array of contiguous equilateral triangles [9]. A schematic of an iso-grid is shown in Figure 1. A cell of a grid structure has three basic components which are rib, node and bay. One of the main advantages of having a grid structure is that crack is not likely to propagate across the ribs improving the damage tolerance of the structure [10]. The strength of the iso-grid structures is derived from their ribs [11]. Another advantage of a grid structure is that the manufacturing process can be automated which would make the manufacturing easier and also reduce the number of imperfections. Low velocity impact has been an epidemic problem in sandwich structures. Low velocity impact would result in interfacial cracks compromising the strength of the structure [12]. Impact can cause internal damage which would result in a significant reduction in the strength of a structure [13]. So characterizing the low velocity impact response of sandwich structures and also their residual strength is important.

The properties of the core can be enhanced by combining two different core materials. For example combining a honey comb core with foam core would improve the mechanical properties of the sandwich structure when compared with that of a regular core [14]. Also, combining of dry ortho-grid with syntactic foam enhanced the properties of the core and also improved the impact resistance of the sandwich structures [15].

Of the three types of grid stiffened structures, only the response of ortho-grid to low velocity impact was studied. Ortho-grid can be used in applications were the direction of the applied load is known where-as because of the quasi-isotropic nature of iso-grid it can also be used where the direction of load is not known. We propose to develop hybrid core iso-grid

stiffened sandwich structure, the core of which consists of glass fibers aligned in the pattern of an iso-grid and the bay area is filled with syntactic foam. This makes the core a hybrid core in which the fiber can transfer the impact energy elastically and the foam can absorb the propagation energy through micro/macro-length scale damage. It was observed that a positive composite action is developed between glass fiber and syntactic foam which make the hybrid core [15]. In this study an iso-grid stiffened sandwich structure with a hybrid core will be fabricated, tested and modeled to study the impact response and residual strength of the iso-grid stiffened sandwich structure.

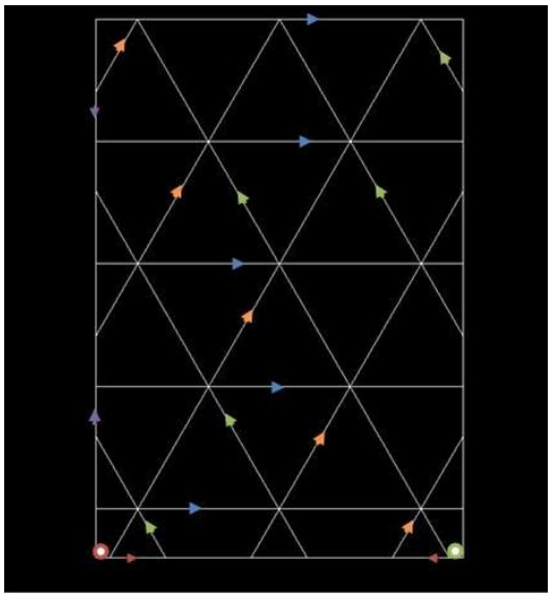

Figure 1.1 Weaving pattern of iso-grid.

In Chapter 2 review of previous work on sandwich structures, grid stiffened structures and laminates are discussed. Fabrication procedure used to manufacture the specimens and the material properties of iso-grid stiffened sandwich structures are given in Chapter 3. Different tests conducted to study the iso-grid stiffened sandwich structures and the results obtained from the tests are discussed in Chapter 4. In Chapter 5 modeling procedure of iso-grid using ANSYS and the results obtained are discussed. Parametric study conducted by varying different

parameters that constitute the iso-grid is discussed in Chapter 6. Conclusions and future work are discussed in Chapter7.

CHAPTER 2. LITERATURE REVIEW

According to American Society for Testing and Materials, syntactic foam is defined as a "material consisting of hollow sphere fillers in a resin matrix". Because of their high strength to weight ratio syntactic foams are being used in wide range of applications. One such an application is foam cored sandwich structures. Many studies were performed on different properties of syntactic foams and their sandwich structures. Voids have been one of the main problems in the fabrication of syntactic foams, so ultrasonic inspection on the foams to determine voids in the foam is important. Different parameters like the volume fraction of glass microballoons, coating of micro-balloons, adding fillers to the core etc affect the properties of sandwich structures. Kim and Kamis [16] studied the effect of volume fraction of glass microspheres on the fracture and impact properties of syntactic foam. Their study showed that impact energy absorption and flexural modulus increased with the increase in volume fraction of glass microspheres up to 0.65. Li and Nji [17] studied the effect of coating the microballoons with rubber latex on both the hybrid syntactic foam and the foam cored sandwich structures. They found that impact energy absorbed by the foam with rubberized glass particles was higher than that absorbed by conventional syntactic foam or pure epoxy. Karthikeyan and Kishore [18] compared the elastic behavior of plain syntactic foams and fiber reinforced syntactic foams and found that the latter has better compressive and specific modulus. The radius ratio of microballoon is an important parameter which affects the compressive strength and modulus of the syntactic foam. The study by Woldesenbet et. al [19] shows that as the radius ratio of the microballoon decreases compressive strength and modulus of the syntactic foam increases. Gupta et. al [20] studied the effect of void content in plain and fiber reinforced syntactic foams. Void content in the foams decrease the compressive strength of the foam. Karthikeyan and

Kishore [21] studied the flexural behavior of fiber reinforced syntactic foams. The addition of fibers resulted in an increase of flexural properties of the syntactic foam.

Sandwich structures have high stiffness and high strength to weight ration. Because of their wide range of applications, determining the mechanical properties of the sandwich structures and their response to damage under different testing conditions is important. Though both core and skin play an important role in the sandwich structures, the study by Akil and Cantwell [22] showed that the dynamic response of the sandwich structures depend on the elastic properties of the core. Vaidya et. al [23] studied the effect of impact damage on partially foam filled honey comb core sandwich structures. Their study showed that addition of foam to the honey comb structures improved the penetration resistance during impact and also an improvement in energy absorption. They also observed that one negative factor influencing the foam filled honey comb core sandwich structures is weight. Lim et. al [24] studied failure modes of foam cored sandwich specimens under static and impact loading using experimental and analytical methods.

Low velocity impact response of the composite sandwich structures is an important factor to be considered. Sjoblom et. al [25] studied the low velocity impact characterization of composites and found that impact force is a better parameter in direct material characterization than impact energy. The study by Ishai et.al [26] showed that the damage tolerance of the sandwich structure would depend on the impact energy but not on the velocity of impact. Belingardi and Vadori [27] studied the impact response of glass fiber epoxy laminates made from unidirectional lamina using different weights and different velocities. They concluded that the saturation impact energy which is the maximum energy that can be absorbed by the material without perforation is the important parameter to be considered. Damage threshold load of

composite laminates was studied by Schoeppner and Abrate [28]. In order to determine the damage threshold loads the impact load should be above the threshold load and the damage threshold load varies with the laminate thickness.

Ultrasonic inspection in foams and sandwich structures is important in order to study the defects in the specimen during fabrication and also to observe the extent of damage when subjected to forces like impact. Ray et. al [29] evaluated the defects in FRP composites using NDT techniques like thermal imaging, ultrasonic (A-scan and C-scan) and SEM. Cosenza et. al [30] conducted non-contact ultrasonic inspection of the bond between the skin and core in honeycomb with lamb waves.

Grid structures which have a particular stiffening arrangement are called grid stiffened structures. Because of their high specific strength, grid stiffened structures are being used in many fields like construction. Li et. al [31] studied the compression properties of FRP cylinders. They showed that the crack propagation is along the direction of fiber except for 0^o ply and fiber orientation affects the material properties and stress-strain behavior. Woldosenbet et. al [32] investigated the buckling problems in grid stiffened cylinders and developed a numerical model which predicts the buckling loads on the grid stiffened cylinders. Experimental study of hybrid composite cylinders by Li [33] showed that grid cylinders have higher specific strength than solid steel tubes and FRP tubes. Li and Velamarthy [34] performed their studies on grid stiffened cylinders and found that grid stiffened cylinders have higher compressive strength, resistance to failure when compared with normal fiber reinforced polymer tubes. They also observed a considerable increase in strength with the addition of fillers to the grid stiffened cylinders. Parametric study was performed by changing skin thickness, rib thickness, bay area and modulus of the skin. A significant effect is observed because of the change in the above mentioned

parameters. Han and Tsai [35] investigated a cost effective procedure to manufacture interlocked composite grid. The comparison of the flexural stiffness of a sandwich panel of same dimensions with that of the interlocked composite grid showed that the interlocked composite grid has better stiffness and the grid is cost effective.

Huybrechts and Tsai [36] observed a change in failure mode in iso-grid structures with rib thickness, thinner rib failed due to buckling whereas the failure of thicker rib was due to material failure. They also observed that the angular ribs give majority of the shear strength to the grid structure. An important conclusion by Huybrechts about iso-grid is that in failure space iso-grid structures are not isotropic. Jadhav and Mantena [37] performed parametric study of quasi-static and dynamic impact with varying rib and skin thickness, rib width and center to center distance between rib joints to optimize the specific energy absorption. Impact loading was given on two different sides which are skin side and rib side. Kidane et. al [38] performed buckling load analysis on iso-grid stiffened cylinder. They developed an analytical model which was validated by an experimental test. Parametric study performed by them showed that the structure with an orientation angle of 42^{o} was able to take higher buckling loads when compared with other orientations. They also observed that the buckling load varies with the winding angle of the skin. Gan et. al [39] studied the energy absorption of grid stiffened composites under transverse loading. Their tests and simulations showed that grid stiffened composites have excellent damage tolerance and most of the energy absorption occurs beyond initial failure. Chen and Tsai [40] compared theoretically the stiffness, strength and hygro-thermal properties of laminate, sandwich and an iso-grid. They used four different materials of T300/5208, E-glass, Steel and Aluminum to compare the properties of the above structures. Iso-grid showed higher flexural strength ratio, in-plane strength ratio with E-glass when compared to laminate and

sandwich. Recently, Li and Cheng [41] developed a new analytical modeling of orthogrid stiffened sandwich structure with or without syntactic foam in the bay area. They modeled this periodic structure without smearing or homogenizing.

The different kinds of cores in sandwich structures are foam core, web core, and integrated core (foam filled in web core) [15]. Even though foam cored sandwich structures absorb energy, they are brittle. Web core lacks of bonding with skin and suffers from skin buckling and web buckling problem as well as having impact windows [15]. Therefore, Li and Muthyala [15] worked on a hybrid core which is a combination of orthogrid and foam core. The hybrid core sandwich structure provided a better elastic response and absorbed higher energy because of the positive composite action. The foam helped in absorption of energy and the grid skeleton helped in stopping the damage propagation due to impact. Their study showed that the samples with half-inch bay area have better impact properties and their residual load carrying capacity is also higher than other groups. Parametric study was performed by considering different parameters like skin thickness, skin modulus, rib width, rib modulus and bay area. There is an increase in the value of the modulus with an increase in skin thickness, skin modulus and rib modulus. For the rib width and bay area there is a decrease in the modulus till a certain point and an increase in the value of modulus is observed.

Though the ortho-grid stiffened structures improved the impact properties and residual strength, their residual strength when impacted at bay which occupies higher percentage area is much lower than node which occupies a small percentage of area. Therefore an iso-grid stiffened sandwich structure is proposed in this study which is in-plane quasi isotropic and has resistance to different forces like tension, compression, shear and flexural loads.

CHAPTER 3. MANUFACTURING AND CHARACTERIZATION

3.1 Raw Materials

The raw materials used in the fabrication of the grid structure are Epoxy DER 332 and curing agent DEH 24 supplied by Dow chemicals, glass microspheres supplied by Potters industries, glass fiber rovings supplied by Saint Gobain, plain woven 7715 style fabric and woven fabric supplied by Fibre Glast. The material properties are listed in Table 3.1. The material properties are taken from the data sheets provided by the manufacturer.

Table 3.1Material properties of raw materials used

Material	Modulus of Elasticity (GPa)	Shear Modulus (GPa)	Poisson's Ratio
Resin	1.81	0.6	0.3
Glass microspheres	75.1	30.6	0.2
E-glass fiber	73.0	29.9	0.2

3.2 Composition of Materials

The core is a hybrid core consisting of an iso-grid skeleton which is filled in by syntactic foam in the bay area. The syntactic foam used in this study is prepared by mixing glass microspheres and resin in the ratio of 60:40 by volume. The resin used in the foam is a mixture of 85% of DER 332 and 15 % of DEH 24 by volume. The composition of syntactic foam is shown in Table 3.2. During the fabrication of iso-grid three different bay areas are considered. The hybrid core is made of glass fiber which is approximately 10% by volume and syntactic foam which is 90% by volume. The values of volume fraction of fiber for the laminate and different bay areas of iso-grid are shown in Table 3.3. In order to maintain the number of rounds

of weaving to be an integer and also to keep the volume fraction of glass fiber to be close the volume fraction of glass fiber was varied for different groups.

Table 3.2 Composition of syntactic foam and amount of each constituent for preparing one sandwich slab

	Volume Fraction (%)	Volume (cm^3)	Density (g/cm^3)	Weight (g)	Weight Fraction (%)
Epoxy Part A	34.0	827.9	1.16	960.4	73.4
Curing Agent	6.0	146.1	0.981	143.3	13
Micro balloons	60.0	1461	0.14	204.5	15.6

Table 3.3 Number of strands and volume fraction of glass fiber

Group No.	Number of Fiber Strands	Volume Fraction (%)	Bay Area (mm^2)
1	-	10.0	-
2	3	11.3	12.7
3,5	4	10.9	25.4
4	5	10.4	50.8

In order to make the number of strands a positive integer, Group 2 and group 3 have fiber volume fractions are slightly higher than 10%. If the number of strands is decreased for Group 2 and 3 the difference in the volume fraction would be much higher. In order to maintain constant fiber volume fraction the rib width has to be varied for different groups depending on the number of strands. Group 1 specimen is a cross-ply laminate which was prepared by using plain woven 7715 style fabric. The fiber volume fraction in Group 1 is close to the grid stiffened sandwich structures. Therefore, Group 1 can be used as a control group.

3.3 Manufacturing Process

The iso-grid was made using a pin guided dry weaving process. A wooden board with 534mm×534mm is taken and pins are pinned around the wooden board based on the geometry of

the iso-grid. The nodal build up is reduced by moving pins of the horizontal rib a few mm downwards. A non-porous Teflon sheet is placed on the wooden board within the pin boundary, in order to avoid the foam coming in contact with the board. A woven roving fabric of appropriate dimensions is cut and placed over the non-porous Teflon sheet to form the bottom skin for the sandwich structure. The mold shown in Figure 3.1 was used for fabricating a Group 3 sample. Along the bottom and top side the pins are placed at a distance of 38.6 mm which is the length of a side of an equilateral triangle. Along the sides the pins are placed at a distance of 33.4mm, which is the height of the triangle. The grid is dry weaved with the help of these pins. For Group 3 samples four strands of fiber are used for one weave of the grid. Once the weaving process is completed, the mold is then placed on the bottom layer of the vacuum bag. Tacky tape was placed around the mold in order to seal the vacuum bag and it helps to maintain vacuum pressure inside the bag.

Syntactic foam is prepared by mixing glass microspheres with the part A. Once the glass microspheres are thoroughly mixed with epoxy, part B which is the curing agent is added to the mixture and mixed. The foam is poured into the grid skeleton as shown in Figure 3.2. A layer of woven roving fabric is placed on the top of the grid with foam as shown in Figure 3.4 and a plastic sheet was placed on top of the skin to avoid the sticking of glass plate to the skin.

A quarter inch thick glass plate was placed on the plastic sheet so that uniform pressure shall be applied on the top layer of the skin and to obtain a smooth surface. The whole setup is placed under vacuum for 24 hours as shown in Figure 3.5. The vacuum process helps in eliminating voids in the sample and also distributed the foam evenly throughout the grid. The sample is cured at room temperature for 24 hours. Then the sample is placed for post curing in the oven for three hours at a temperature of 100^{o}C.The specimens were cut to 150mm×100mm

using a precision cutter. The specimens were cut such that they are symmetric about the y-axis as shown in Figure 3.3.

3.4 Burn-Out Test

ASTM D2584- Standard Test Method for Ignition Loss of Cured Reinforced Resins was used to perform the burn-out test. Burn-out test was performed on the rib, node and skin of the specimens from Groups two to four in order to determine the volume fraction of the fiber at the corresponding locations. Burn-out test is performed on the Group 1 specimens on the skin and the inner layers of the laminate to determine corresponding volume fractions. Small pieces are cut from ribs, node and skin. The samples are taken in a crucible and the weight of the crucible and the weight of the crucible with the sample are recorded. The crucible with the sample is then placed in an oven and was heated at a temperature of 565 degrees centigrade for about two hours until the resin is completely burned. The weight of the crucible with sample after burn out is recorded and the weight fractions and volume fractions of the fiber, microballoons and resin are obtained. The following procedure was used to calculate the volume fractions.

W_c= Weight of the crucible

W_{c+s}= Weight of the crucible + Weight of the sample

W_{c+s-r}= Weight of the sample after burn out

Wr= Weight of resin

W_f= Weight fraction of resin (W_r/W_s)

Table 3.4 Calculation of volume fractions

	Volume fraction	Density (g/c.c)	Weight (g)	Weight fraction
Resin	0.4ν	1.16	0.464ν	0.464ν/2.72-2.172ν
Glass Microballoons	0.6ν	0.14	0.084ν	0.084ν/2.72-2.172ν
E-glass Fiber	1-ν	2.72	2.72-2.72ν	2.72(1-ν)/2.72-2.172ν
Sum	1		2.72-2.172ν	1

For samples from group 2 to 5 burn out test is performed at rib, node and skin. For samples of group 1 the test is performed for the inner layers and the outer layer. For Groups 2, 3 and 4 the volume fraction of fiber at rib is 24% where as for group 5 the value is 28%. The volume fraction of fiber at node for group2 is 69%, for group 3 and 4 is 72%, for group 4 is 80%. The volume fraction of fiber for the skin is 61% for group 2 to group 5. For the laminate the percentage of volume fraction of fiber are 37 and 60 for the inner and outer layers respectively.

Figure 3.1 Wooden mold with pins and bottom skin

Figure 3.2 Foam is being poured into the grid skeleton

Figure 3.3 A sample showing how the specimens are cut


Figure 3.4 Top layer of the skin placed on the grid skeleton filled with foam

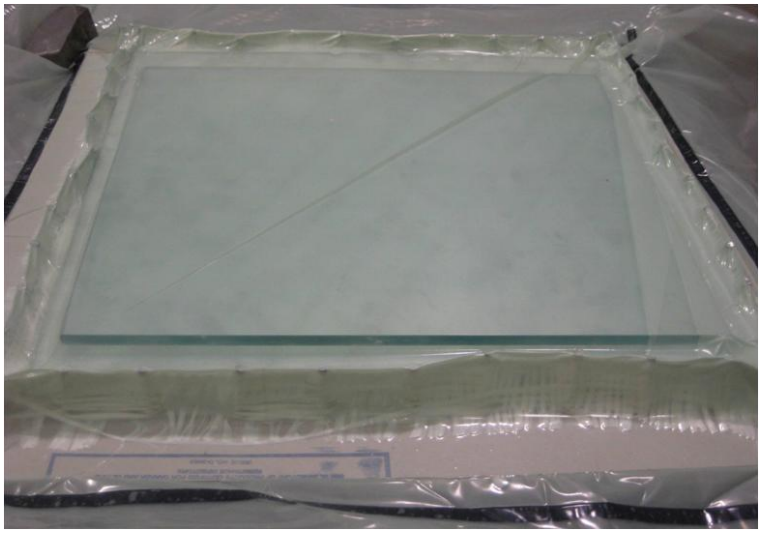
Figure 3.5 Mold placed under vacuum

3.5 Determination of Mechanical Properties

The mechanical properties of the iso-grid sandwich structure are calculated using the volume fractions of the fiber and matrix at different locations for different groups. The values of Young's Modulus, Shear Modulus and Poisson's ratio are calculated using the rule of mixtures. The values of Poisson's ratio for the node and skin are calculated using equation 3.2. The strains in equation 3.2 are obtained from the coupon test performed on the ribs of the samples from Groups 2, 3 and 4. These mechanical properties are used in performing Finite Element Analysis of the models using ANSYS. Rule of Mixtures and Halpin-Tsai equations are used in determining the mechanical properties. Tables 3.5 – 3.9 shows the material properties of specimens with different bay areas. The porosity values of Groups 1-5 are shown in Table 3.11. The percentage area occupied by bay, node and rib is shown in Table 3.12.

$$E1 = EfVf + EmVm \quad (3.1)$$

$$\nu 12 = -\frac{\epsilon 2}{\epsilon 1} \quad (3.2)$$

$$\frac{1}{G12} = \frac{Vf}{Gf} + \frac{Vm}{Gm} \quad (3.3)$$

$$\frac{Ef}{Em} = \frac{1+\xi\eta Vf}{1-\eta Vf} \quad (3.4)$$

$$\eta = \frac{\frac{Ef}{Em-1}}{\frac{Ef}{Em+\xi}} \quad (3.5)$$

Where; V_f= Volume fraction of the fiber

V_m= Volume fraction of the matrix

E_f= Elastic modulus of the fiber

E_m= Elastic modulus of the matrix

ν_f= Poisson's ratio of the fiber

ν_m= Poisson's ratio of the matrix

G_f= Shear modulus of the fiber

G_m= Shear modulus of the matrix

ξ= 2 for circular fibers

Table 3.5 Material properties of Group 1 specimens

	Inner plys	Outer layers
E_1	12047	24619
E_2	1829	24619
E_3	1829	2855
G_{12}	715	1117
ν_{12}	0.264	0.261

Table 3.6 Material Properties of Group 2 specimens

	Rib	Node	Skin
E_1	11902	27097	23966
E_2	1615	27097	23966
E_3	1615	3560	2852
G_{12}	631	1393	1115
ν_{12}	0.335	0.26	0.261

Table 3.7 Material properties of Group 3 specimens

	Rib	Node	Skin
E_1	11084	25949	22229
E_2	1613	25949	22229
E_3	2315	3810	2842
G_{12}	630	1491	1111
ν_{12}	0.251	0.258	0.261

Table 3.8 Material properties of Group 4 specimens

	Rib	Node	Skin
E_1	10597	29792	24619
E_2	1529	29792	24619
E_3	1529	4200	2855
G_{12}	597	1644	1117
ν_{12}	0.439	0.28	0.28

Table 3.9 Material properties of 101.6mm^{2}bay area specimen

	Rib	Node	Skin
E_1	10439	32152	24618
E_2	1504	32152	24618
E_3	1504	4255	2855
G_{12}	584	1685	1116
ν_{12}	0.44	0.26	0.26

Table 3.10 Percentage of volume fraction of fiber and foam at different locations

		Volume fraction of fiber (%)	Volume fraction of foam (%)
Group 1	Inner layers	0.30	0.69
	Skin	0.61	0.39
Group 2	Skin	0.61	0.39
	Node	0.69	0.31
	Rib	0.29	0.71
Group 3, 5	Skin	0.61	0.39
	Node	0.72	0.28
	Rib	0.29	0.71
Group 4	Skin	0.61	0.39
	Node	0.74	0.26
	Rib	0.26	0.75

Table 3.11 Percentage of porosity of different Groups

Group	Porosity (%)	Standard Deviation
1	3.79	0.37
2	4.2	0.51
3	5.2	0.49
4	2.91	0.16
5	4.2	0.51

Table 3.12 Percentage area occupied by bay, node and rib

Group	% area of bay	% area of rib	% area of node
2	61	34.1	4.9
3	66.1	30.2	3.7
4	73.2	24.2	2.6

CHAPTER 4. TESTING AND ANALYSIS

4.1 Testing

Low velocity impact characterization and residual strength have been one of the important aspects to be analyzed for composite sandwich structures. Low velocity impact test, Ultrasonic C-scan testing before and after impact, compression test of the specimens before and after impact at various locations were conducted.

4.1.1 Impact Testing

Low velocity impact testing is performed using Instron Dynatup 8250. Impulse Data Acquisition software is used to acquire the data from the machine. Load vs. time and energy vs. time plots are acquired by the software which are used in calculating the initiation energy, propagation energy and maximum load carried by the specimen. Initiation energy is the energy at the maximum load which can be obtained from the energy and load vs. time curve. Initiation energy represents the amount of energy transferred elastically by the target. Propagation energy is the difference between the maximum impact energy and the initiation energy [17]. Propagation energy represents the amount of energy absorbed by the specimen. The length, width and thickness of the specimen are 152.4 mm, 101.6 mm and 15.2 mm respectively. The specimens are subjected to impact at three different locations of bay, node and rib on the iso-grid stiffened sandwich structure. The impact testing was performed at two different velocities of 3m/s and 4m/s with a hammer weight of 24.09kg. A hammer weight of 41.33kg is also used at a velocity of 4m/s. The energies at which the impact test is performed are 108 joules, 192 joules and 330 joules, respectively. Instron Dynatup 8250 used for conducting the impact tests is as shown in Figure 4.1.

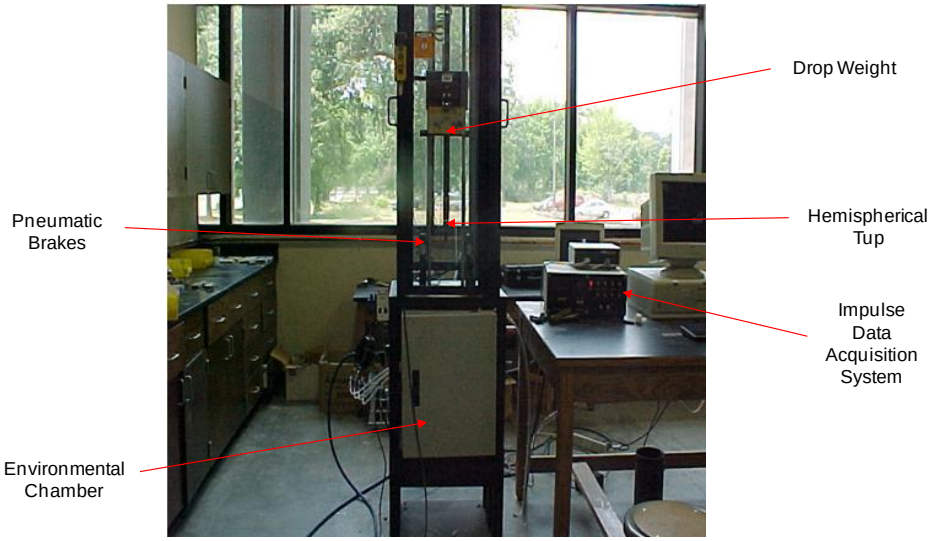

Figure 4.1 Instron Dynatup 8250 impact testing machine

4.1.2 Ultrasonic Inspection

Ultra PAC inspection machine from Physical Acoustics Corporation is used to perform ultrasonic inspection on the specimens before and after impact. A 1MHz transducer acquires the signal from the specimen and is transferred to the computer. Ultra Win software converts the signal from the transducer to C-scan images. The machine used for testing is shown in Figure 4.2.

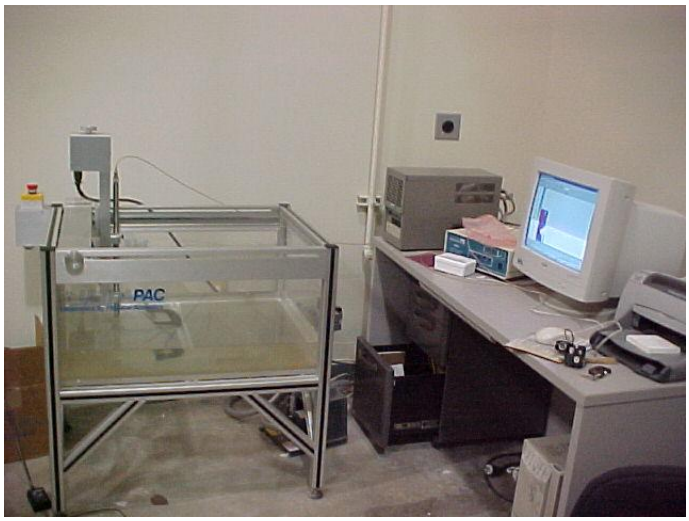

Figure 4.2 Ultrasonic testing machine used to perform C-scan

4.1.3 Compression Testing

MTS 810 machine is used to perform compression after impact test on the iso-grid specimens. The specimen is placed in a "Boeing compression after impact compression test fixture" while conducting the compression after impact test. Compression test was performed on the specimens before and after impact and the values of the modulus are computed. The length, width and thickness of the specimen are 152.4 mm, 101.6 mm and 15.2 mm respectively. The test was performed by strain controlled testing method with a loading rate of 1.3 mm/min.

4.2 Results and Discussion

4.2.1 Impact Testing

A typical load vs. time and Energy-Time curve of a Group 2 specimen subjected to impact energy of 108J at node is shown in Figure 4.4. The blue curve shown in the figure represents energy vs. time and the green curve represents load vs. time. Group 3 specimens impacted at different locations of node, bay and rib with impact energy of 192J are shown in Figures 4.5 - 4.7.

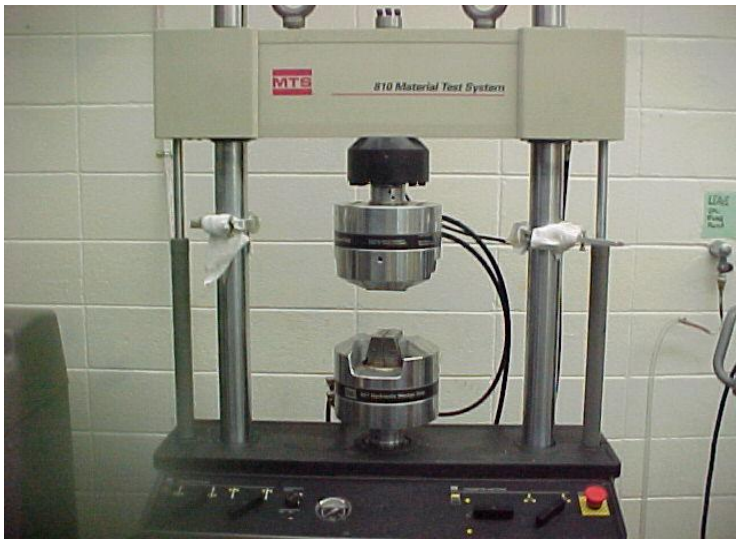

Figure 4.3 MTS 810 Compression Testing Machine

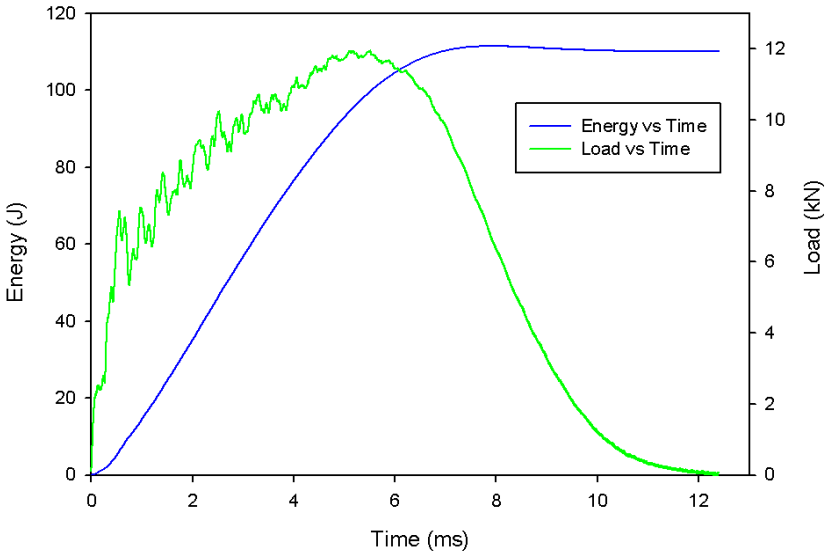

Figure 4.4 Load vs. time and energy vs. time curve of a Group 2 specimen subjected to impact energy of 108J

Figure 4.5 Group 1 specimen impacted at node with energy of 192J

Figure 4.6 Group 1 specimen impacted at bay with energy of 192J

Figure 4.7 Group 1 specimen impacted at rib with energy of 192J

Table 4.1 Impact test results of the specimens subjected to an impact energy of 108J

Group	Location	Initiation Energy (J)		Propagation Energy (J)		Maximum Load (kN)	
		Average	Standard Deviation	Average	Standard Deviation	Average	Standard Deviation
1	Center	70.11	3.75	40.01	3.96	8.47	0.23s
2	Bay	28.04	0.53	73.67	1.37	5.76	0.26
	Node	95.65	4.39	18.64	8.06	11.63	0.30
	Rib	88.3	3.54	30.96	9.64	9.43	0.24
3	Bay	32.91	1.62	75.59	6.01	7.5	0.41
	Node	96.08	0.35	19.6	0.85	13.65	0.89
	Rib	67.55	5.06	43.26	5.86	9.56	0.17
4	Bay	47.48	0.59	58.14	2.27	6.3	0.07
	Node	88.34	3.69	21.66	3.82	8.89	0.72
	Rib	71.15	5.75	41.45	8.27	7.93	0.33
5	Bay	38.66	0.49	77.23	7.16	7.96	0.48
	Node	95.37	3.06	11.77	4.72	12.67	0.46
	Rib	61.26	2.94	48.10	2.19	8.8	0.27

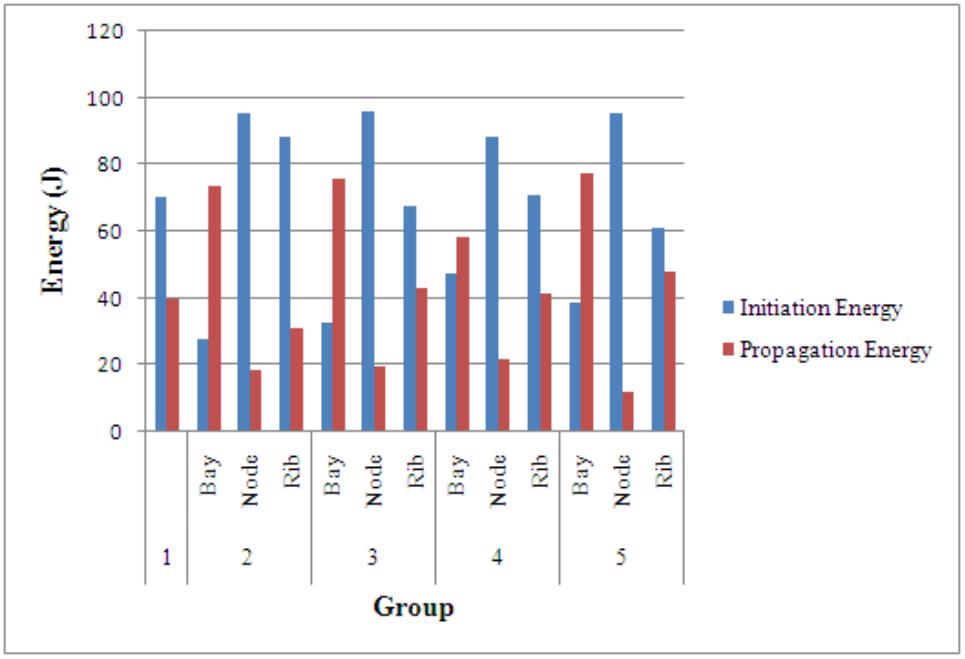

Figure 4.8 Initiation energy and Propagation energy with impact energy of 108J

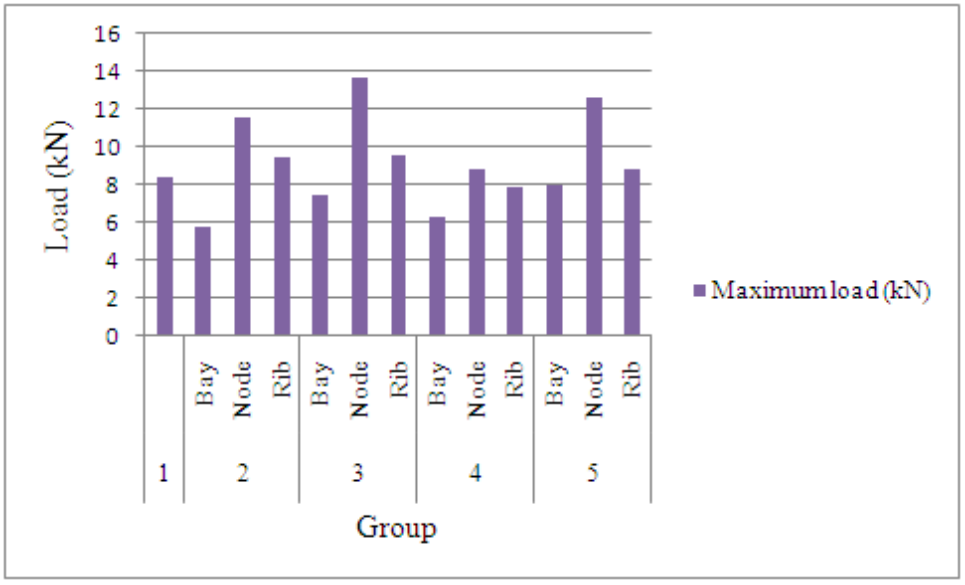

Figure 4.9 Variation of maximum load for the specimens subjected to impact energy of 108J

The values of initiation energy, propagation energy and maximum load obtained by subjecting the specimens with impact energy of 108J are given in Table 4.1. The initiation energy is highest at the node location for Group 3 specimens subjected to impact energy of 108J. The propagation energy is highest for a Group 5 specimens impacted at bay. Impact at node for

Group 3 specimens leads to the highest maximum impact force. Figure 4.8 compares the values of initiation energy and Figure 4.9 compares the values of maximum load propagation energy of Groups 1-5 subjected to impact energy of 108J. From the figure it can be observed that node location has higher initiation energy and lower propagation energy when compared to bay and rib locations. The reason for this is that the nodes are the point of intersection of the fibers and fiber is a stiffer material which results in a higher load value for crack initiation. On the other hand, the bay area lacks fiber reinforcement, leading to the highest propagation energy and lowest initiation energy values. Impact at ribs leads to the values of initiation energy and propagation energy in between that of bay and node.

Table 4.2 Impact test results of the specimens subjected to an impact energy of 192J

Group	Location	Initiation Energy (J)		Propagation Energy (J)		Maximum Load (kN)	
		Average	Standard Deviation	Average	Standard Deviation	Average	Standard Deviation
1	Center	112.87	7.78	62.8	8.35	9.65	0.25
2	Bay	59.91	1.62	124.01	3.68	8.42	0.32
	Node	108.59	12.16	80.19	8.68	11.92	1.05
	Rib	80.79	0.35	101.36	1.40	8.73	0.13
3	Bay	44.07	3.33	131.76	6.06	6.5	0.39
	Node	149.53	3.18	39.65	2.7	12.4	0.72
	Rib	76.34	8.28	113.09	7.28	8.18	0.04
4	Bay	57.63	4.65	113.92	5.18	8.44	0.42
	Node	114.57	4.76	74.64	4.36	13.4	0.56
	Rib	82.08	3.00	105.16	2.68	9.02	0.4
5	Bay	48.06	3.33	124.82	6.06	6.5	0.39
	Node	144.25	3.18	46.91	2.7	12.4	0.72
	Rib	74.57	8.28	98.61	7.28	8.18	0.04

The values of initiation energy, propagation energy and maximum load obtained by subjecting the specimens to impact energies of 192J are given in Table 4.2. The initiation energy

is the highest at the node location for Group 3 specimens subjected to impact energy of 192J. The propagation energy is highest for Group 3 specimens impacted at bay. Group 5 nodes have the highest value for maximum load. The values of initiation and propagation energy at node, bay and ribs for the impact energy of 192J followed the same trend as the values for the specimens subjected to impact energy of 108J. The only change observed is the maximum impact force, which occurs at the node of Group 5, instead of Group 3 as in the case of 108J. Figure 4.10 compares the values of initiation energy and propagation energy and Figure 4.11 compares the values of maximum load when the impacted with energy of 192J for Groups 1-5.

The values of initiation energy, propagation energy and maximum load obtained by subjecting the specimens to impact energy of 330J are summarized in Table 4.3. The initiation energy at the node is the highest for Group 4 specimens. The propagation energy is the highest for Group 5 specimens impacted at bay. Group 4 nodes have the highest maximum load value. The values of initiation and propagation energy at node, bay and ribs for the impact energy of 330J followed the same trend as the values of the specimens when they are subjected impact energies of 108J and 192J i.e., the node is basically the strongest component which has the highest initiation energy and lowest propagation energy. This tendency is followed by impact at rib. When the impact is at the bay, the specimens show the highest propagation energy and lowest initiation energy, suggesting that the bay is weakest in revisiting impact damage. Figure 4.12 compares the values of initiation energy and propagation energy and Figure 4.13 compares the values of maximum load when the specimens are impacted with an impact energy of 330J for Groups 1-5.

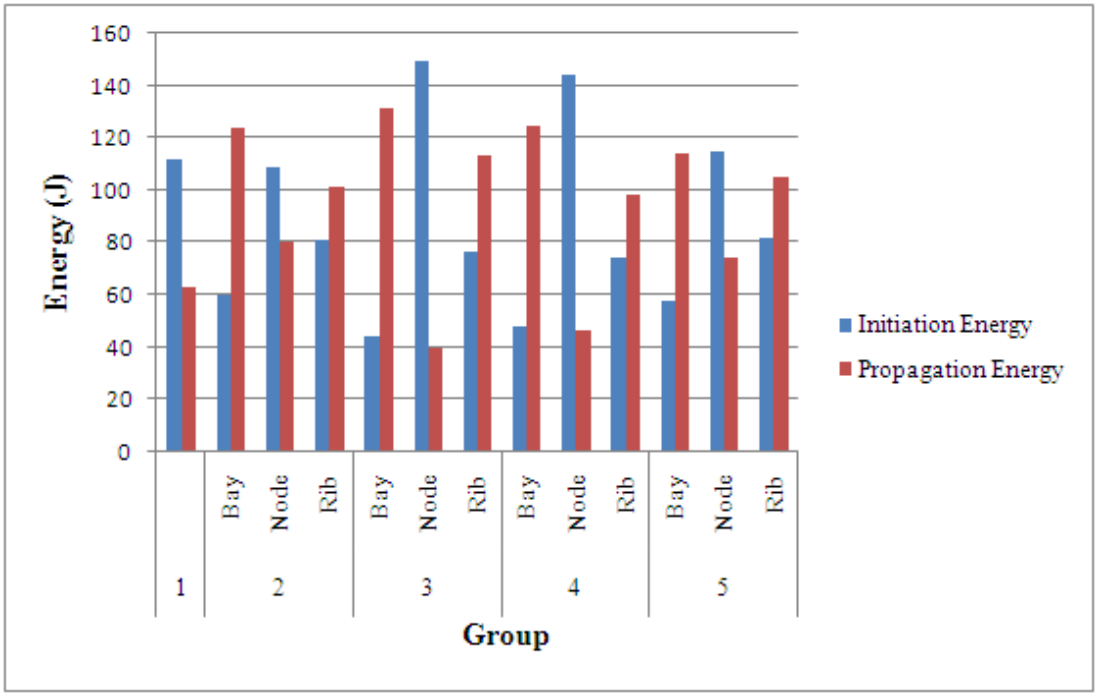

Figure 4.10 Initiation energy and propagation energy with impact energy of 192J

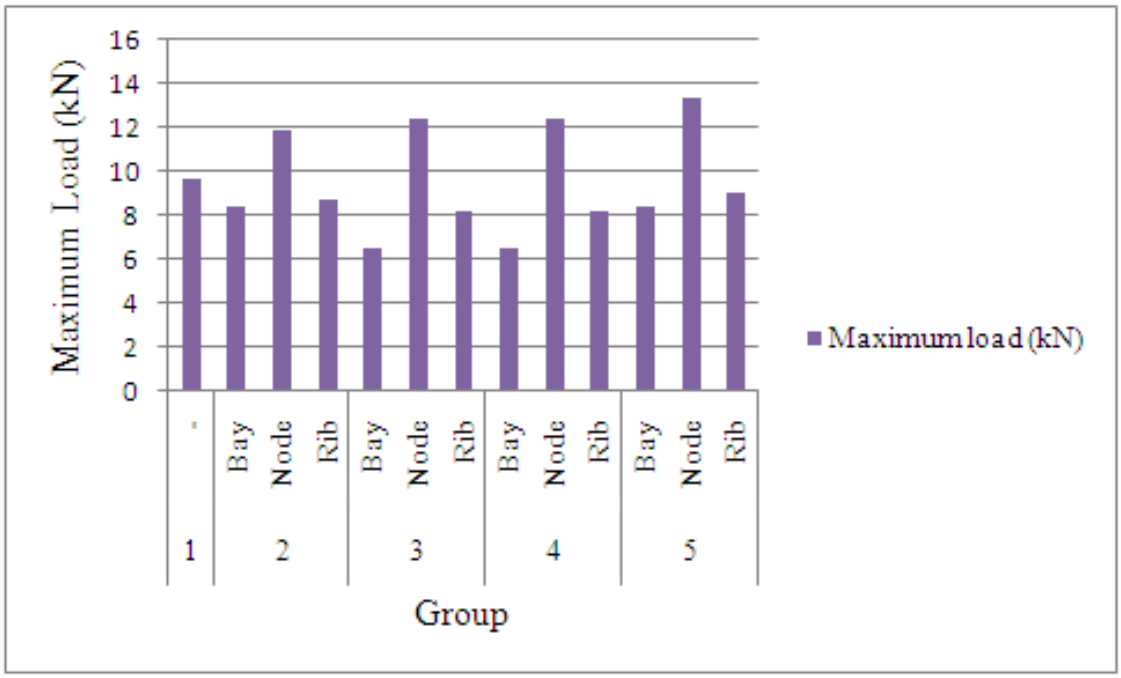

Figure 4.11 Variation of maximum load for the specimens subjected to impact energy of 192J

Table 4.3 Impact test results of the specimens subjected to an impact energy of 330J

Group	Location	Initiation Energy (J)		Propagation Energy (J)		Maximum Load (kN)	
		Average	Standard Deviation	Average	Standard Deviation	Average	Standard Deviation
1	Center	136.05	3.05	161.67	8.35	8.98	0.53
2	Bay	94.54	9.08	195.73	3.34	19.71	0.82
	Node	222.22	6.39	96.94	4.92	22.08	2.01
	Rib	126.19	2.89	165.6	7.5	20.04	3.03
3	Bay	89.21	1.53	206.43	2.73	15.68	0.48
	Node	209.11	9.21	91.27	7.19	19.67	0.72
	Rib	132.42	2.76	160.25	4.37	16.97	1.15
4	Bay	84.28	2.68	201.85	2.23	15.15	1.49
	Node	247.38	6.91	71.97	9.59	21.89	0.84
	Rib	106.02	0.90	190.41	0.72	15.78	2.31
5	Bay	83.72	4.58	209.27	4.92	16.69	2.26
	Node	215.19	6.59	103.96	3.96	19.52	1.22
	Rib	145.86	1.62	162.04	6.11	16.46	1.36

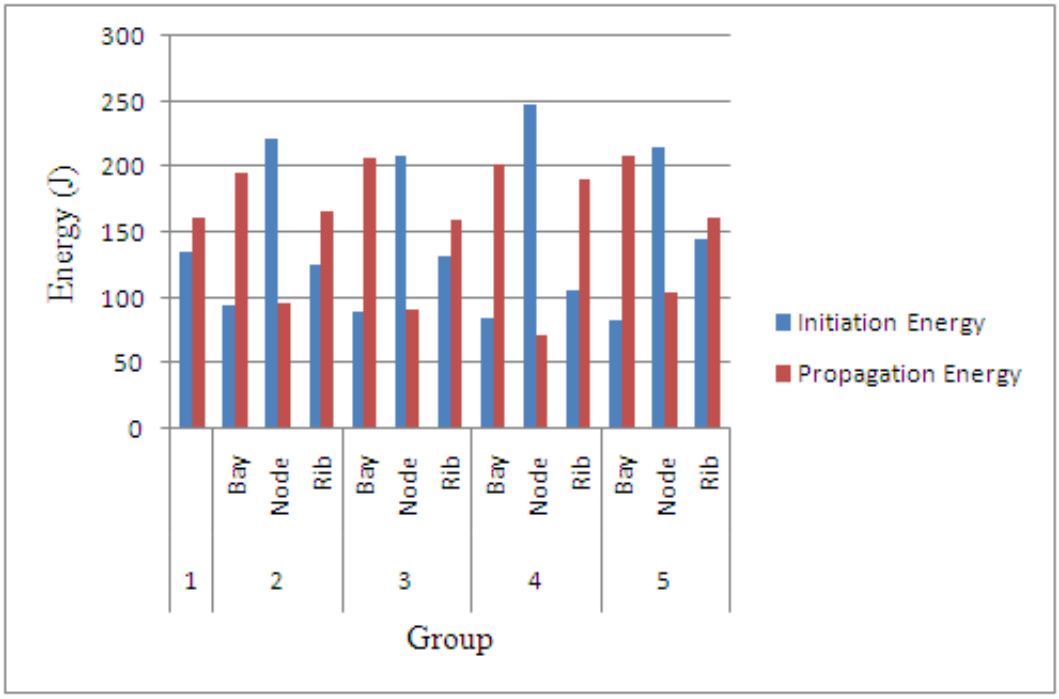

Figure 4.12 Initiation energy and propagation energy with impact energy of 330J

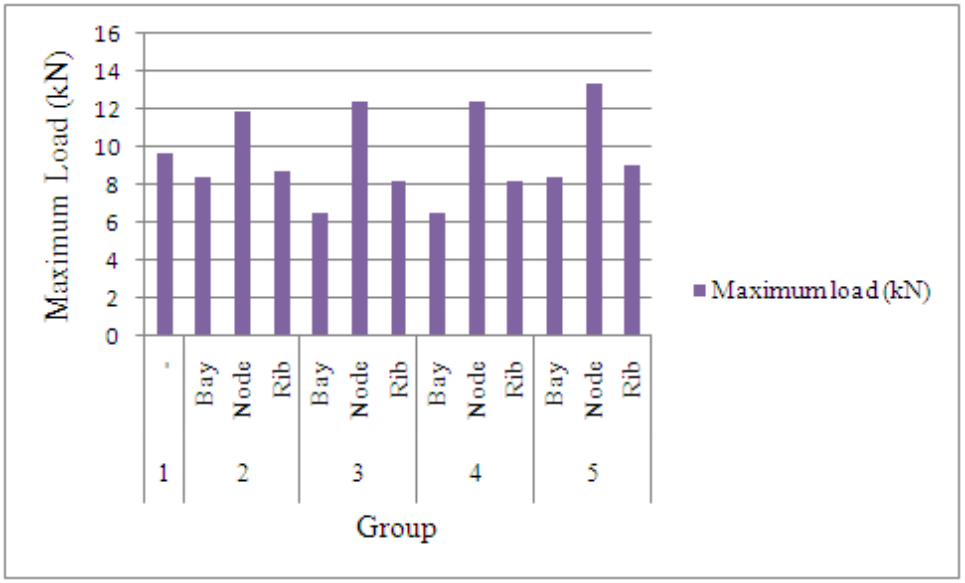

Figure 4.13 Variation of maximum load for the specimens subjected to impact energy of 330J

4.2.2 Ultrasonic Inspection

Pulse-echo transmission method was used to perform C-scan. Depending on the strength of the signal different colors were observed on the C-scan image. Red color represents an excess of 80% of the signal being received by the receiver. Blue color represents 50-80% of the signal being received. Green color represents less than 50% of the signal being received. The settings for each specimen are kept constant while performing the C-scan for pre and post impact specimens. The red region depicts the region with the foam. The blue region depicts the region with fiber. The C-scan images of pre and post impact for all the groups are shown in Figures 4.14 to 4.50. It is observed as the impact energy increases, the area of damage increases.

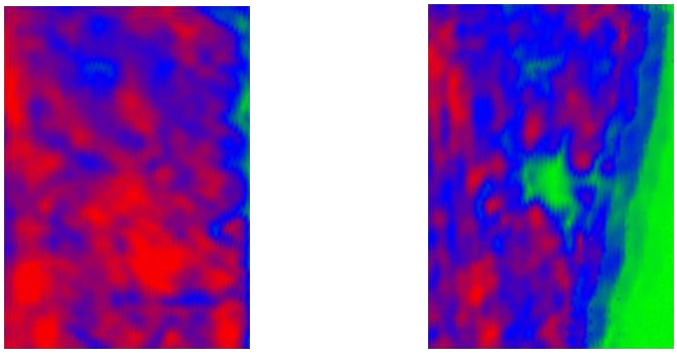

(a) (b)

Figure 4.14 (a) Pre and (b) post impact C-scan image of Group 1 specimen with impact energy of 108J at center

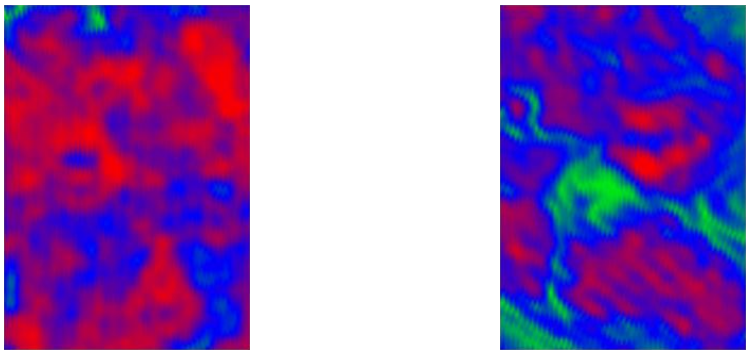

(a) (b)

Figure 4.15 (a) Pre and (b) post impact C-scan image of Group 1 specimen with impact energy of 192J at center

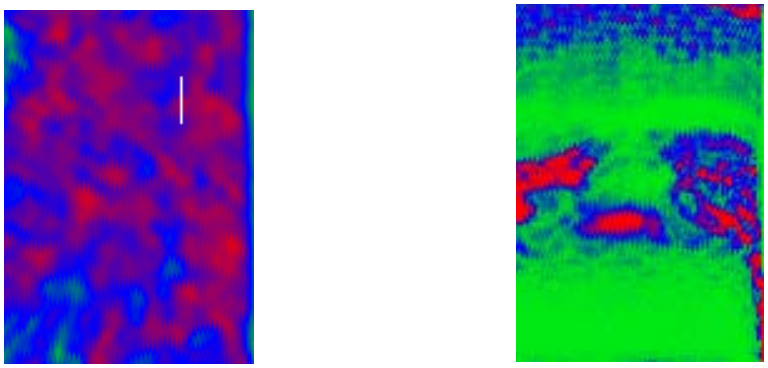

(a) (b)

Figure 4.16 (a) Pre and (b) post impact C-scan image of Group 1 specimen with impact energy of 330J at center

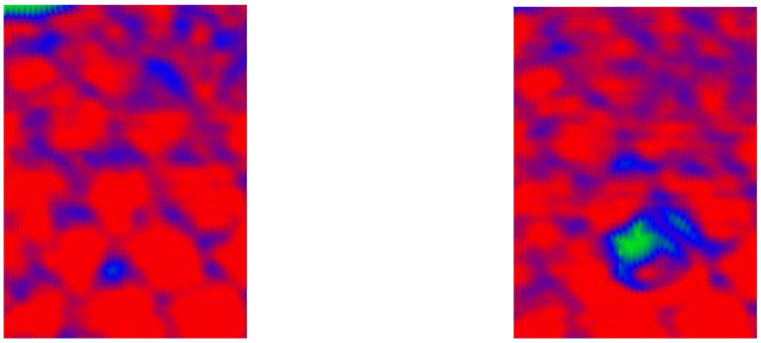

(a) (b)

Figure 4.17 (a) Pre and (b) post impact C-scan image of Group 2 specimen with impact energy of 108J at node

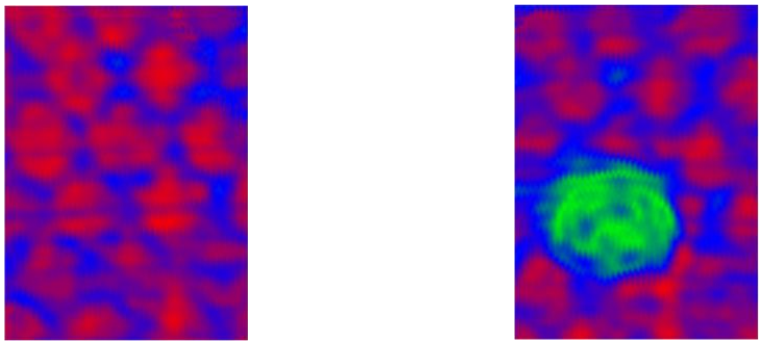

(a) (b)

Figure 4.18 (a) Pre and (b) post impact C-scan image of Group 2 specimen with impact energy of 192J at node

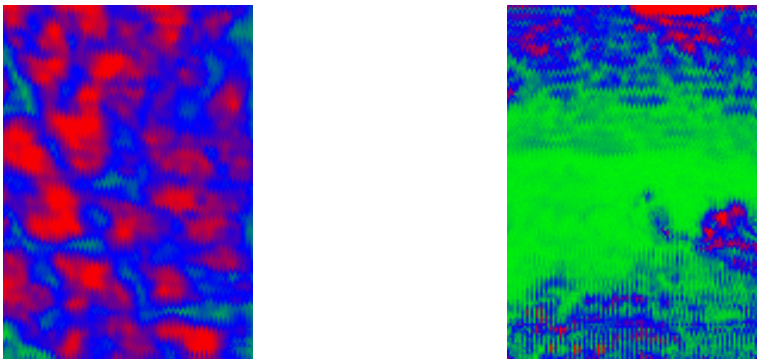

(a) (b)

Figure 4.19 (a) Pre and (b) post impact C-scan image of Group 2 specimen with impact energy of 330J at node

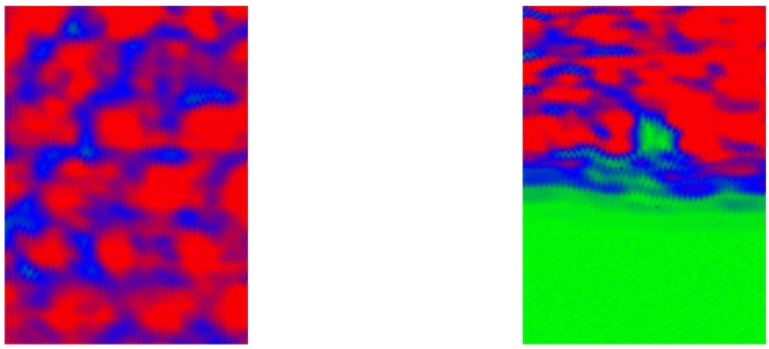

(a) (b)

Figure 4.20 (a) Pre and (b) post impact C-scan image of Group 2 specimen with impact energy of 108J at bay

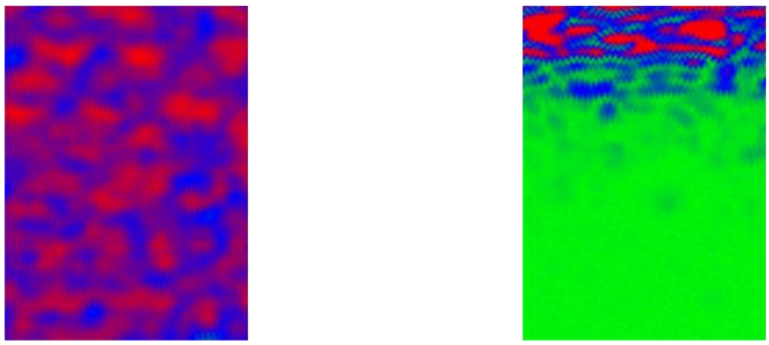

(a) (b)

Figure 4.21 (a) Pre and (b) post impact C-scan image of Group 2 specimen with impact energy of 192J at bay

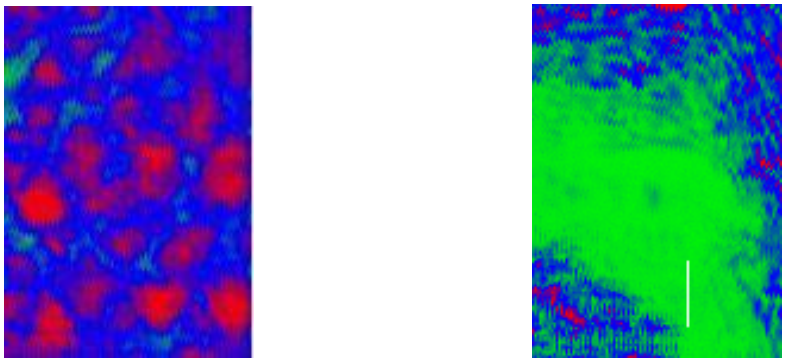

(a) (b)

Figure 4.22 (a) Pre and (b) post impact C-scan image of Group 2 specimen with impact energy of 330J at bay

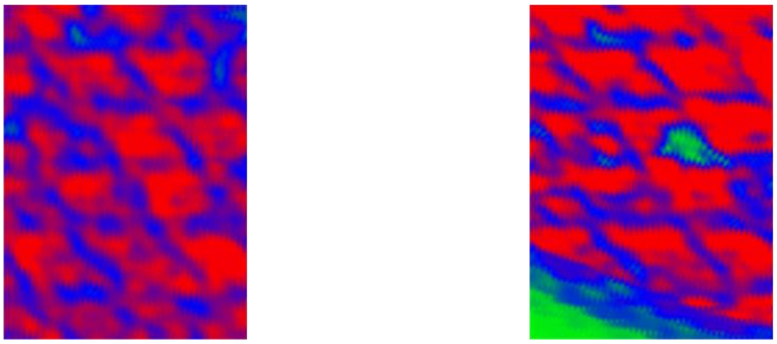

(a) (b)

Figure 4.23 (a) Pre and (b) post impact C-scan image of Group 2 specimen with impact energy of 108J at rib

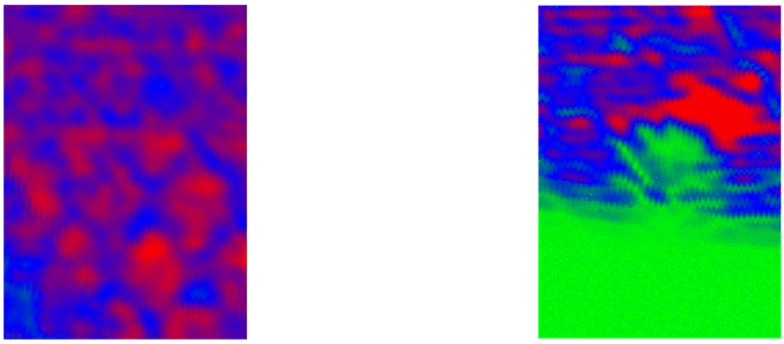

(a) (b)

Figure 4.24 (a) Pre and (b) post impact C-scan image of Group 2 specimen with impact energy of 192J at rib

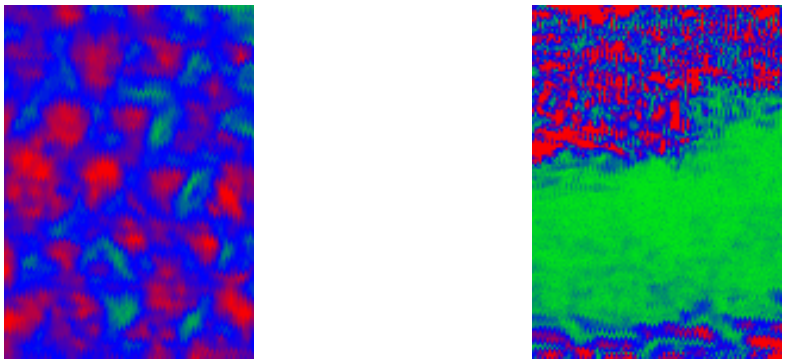

(a) (b)

Figure 4.25 (a) Pre and (b) post impact C-scan image of Group 2 specimen with impact energy of 330J at rib

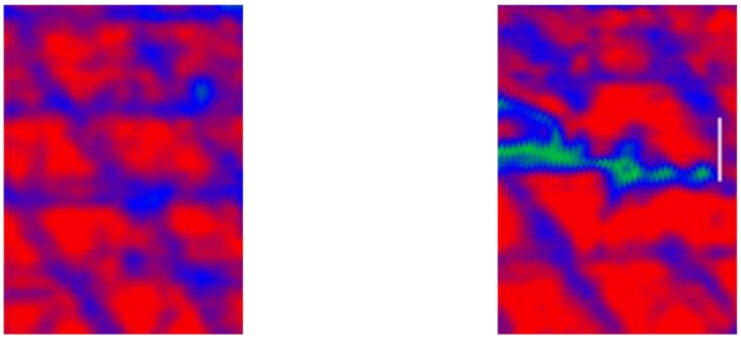

(a) (b)

Figure 4.26 (a) Pre and (b) post impact C-scan image of Group 3 specimen with impact energy of 108J at node

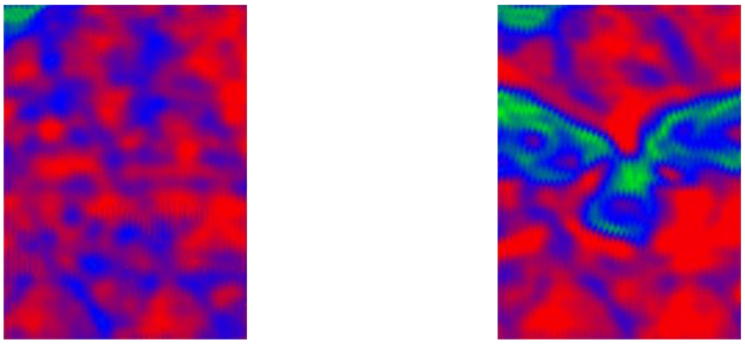

(a) (b)

Figure 4.27 (a) Pre and (b) post impact C-scan image of Group 3 specimen with impact energy of 192J at node

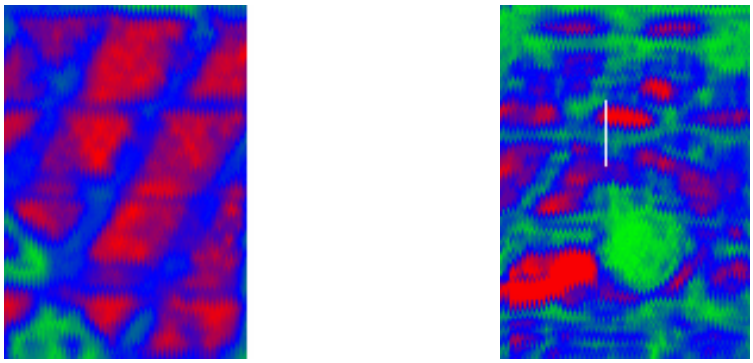

(a) (b)

Figure 4.28 (a) Pre and (b) post impact C-scan image of Group 3 specimen with impact energy of 330J at node

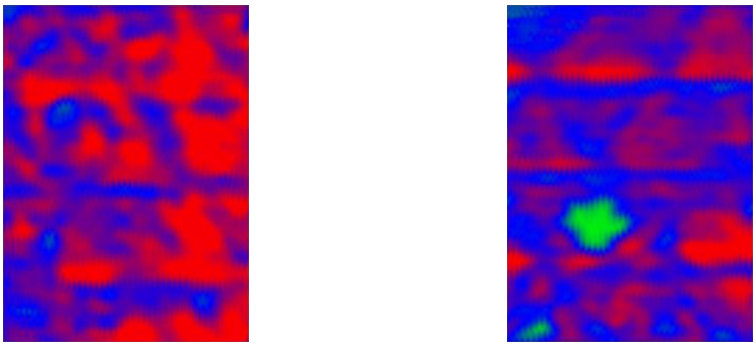

(a) (b)

Figure 4.29 (a) Pre and (b) post impact C-scan image of Group 3 specimen with impact energy of 108J at bay

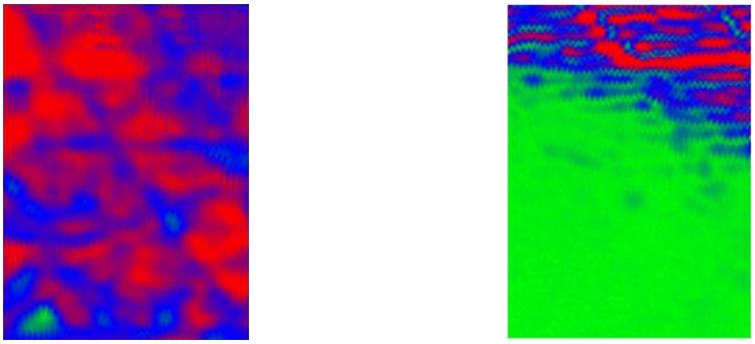

(a) (b)

Figure 4.30 (a) Pre and (b) post impact C-scan image of Group 3 specimen with impact energy of 192J at bay

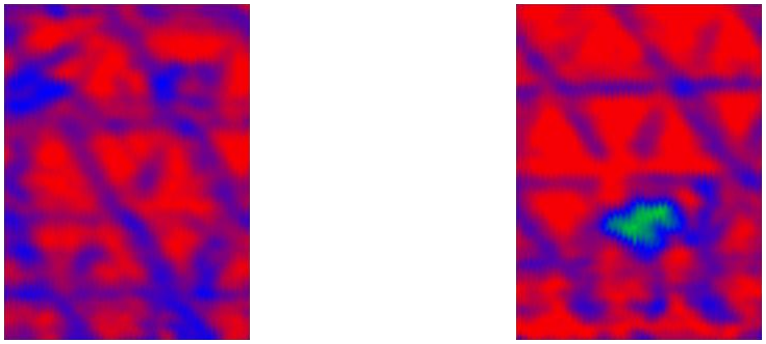

(a) (b)

Figure 4.31 (a) Pre and (b) post impact C-scan image of Group 3 specimen with impact velocity 108J at rib

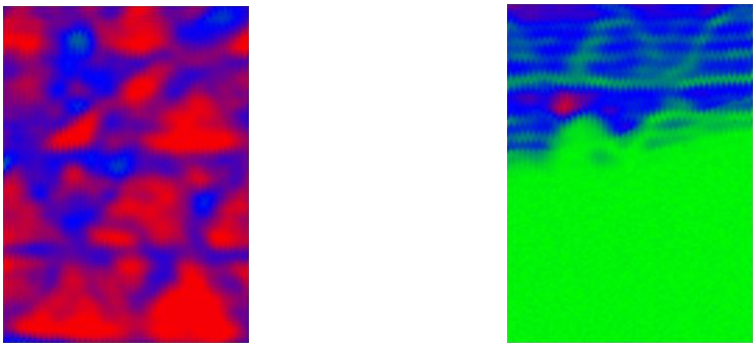

(a) (b)

Figure 4.32 (a) Pre and (b) post impact C-scan image of Group 3 specimen with impact energy of 192J at rib

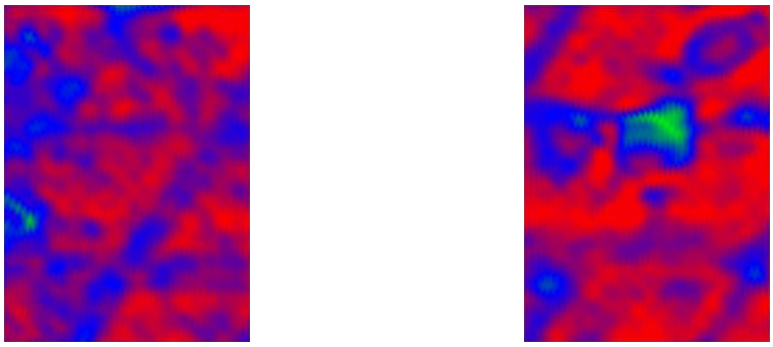

(a) (b)

Figure 4.33 (a) Pre and (b) post impact C-scan image of Group 4 specimen with impact energy of 108J at node

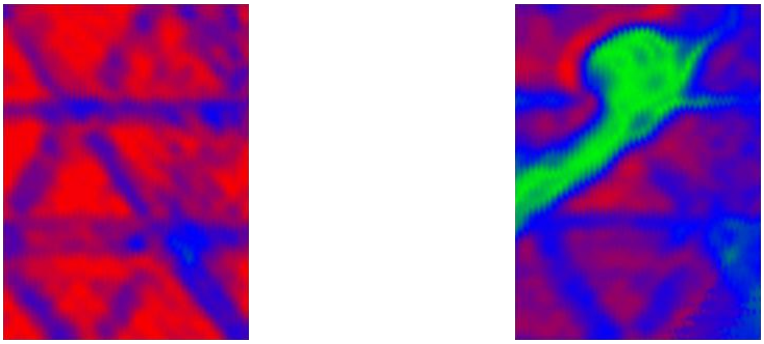

(a) (b)

Figure 4.34 (a) Pre and (b) post impact C-scan image of Group 4 specimen with impact energy of 192J at node

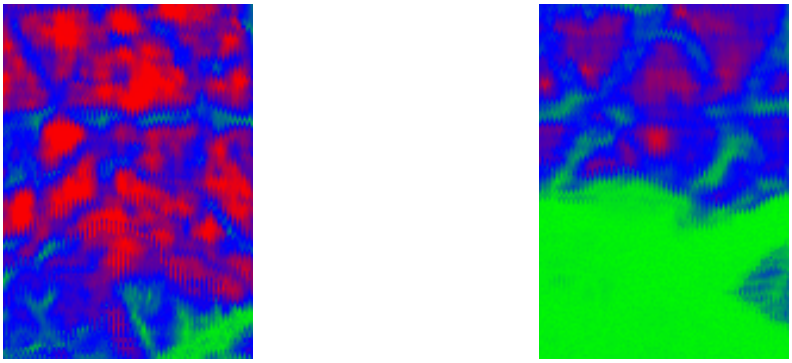

(a) (b)

Figure 4.35 (a) Pre and (b) post impact C-scan image of Group 4 specimen with impact energy of 330J at node

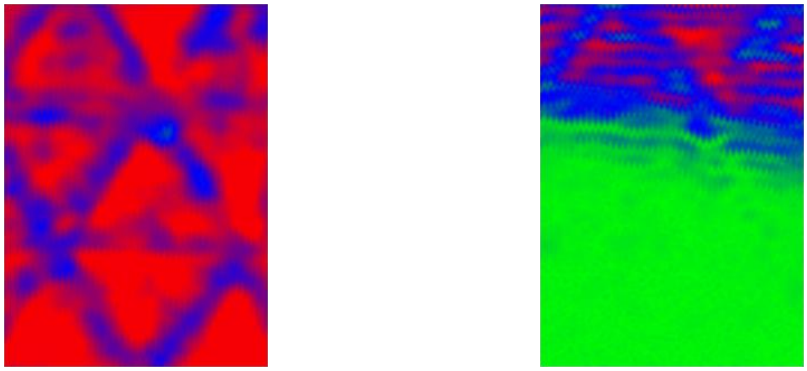

(a) (b)

Figure 4.36 (a) Pre and (b) post impact C-scan image of Group 4 specimen with impact energy of 108J at bay

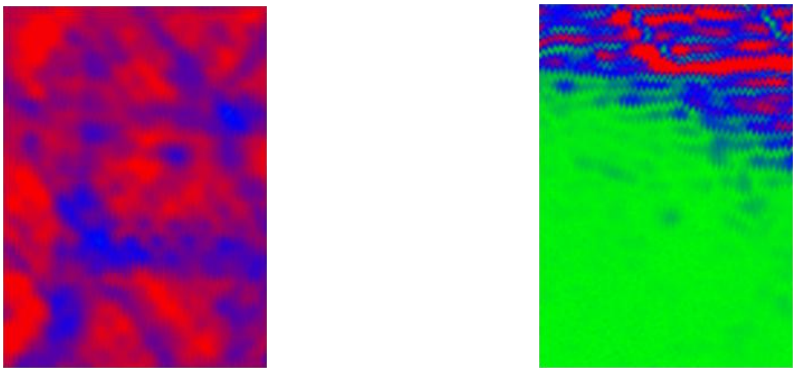

(a) (b)

Figure 4.37 (a) Pre and (b) post impact C-scan image of Group 4 specimen with impact energy of 192J at bay

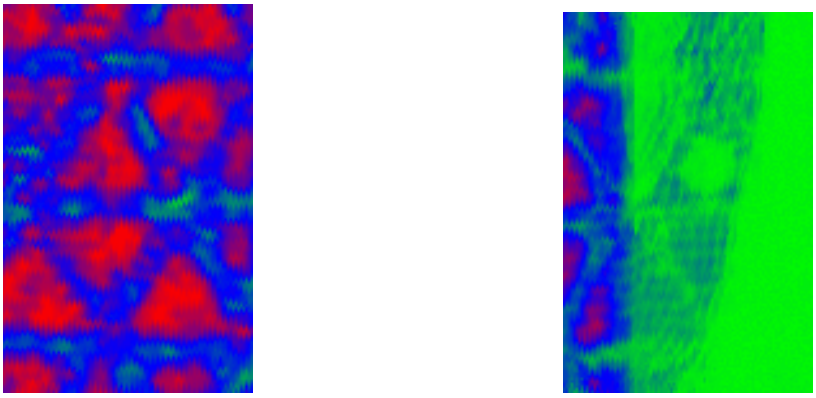

(a) (b)

Figure 4.38 (a) Pre and (b) post impact C-scan image of Group 4 specimen with impact energy of 330J at bay

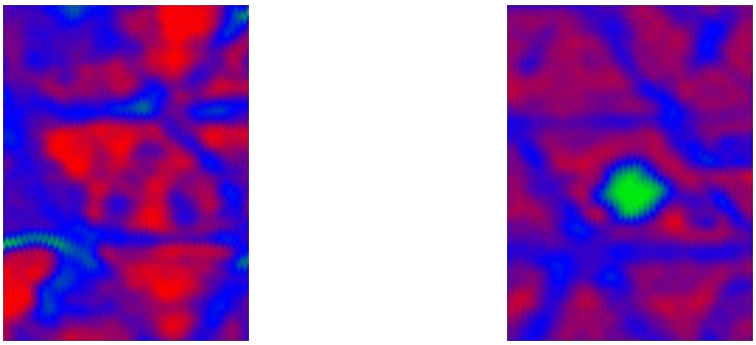

(a) (b)

Figure 4.39 (a) Pre and (b) post impact C-scan image of Group 4 specimen with impact energy of 108J at rib

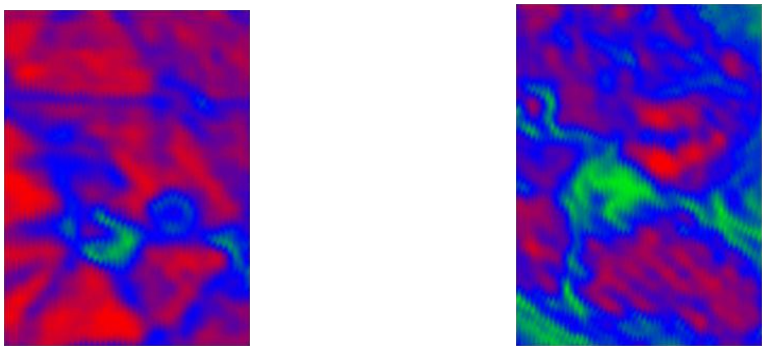

(a) (b)

Figure 4.40 (a) Pre and (b) post impact C-scan image of Group 4 specimen with impact energy of 192J at rib

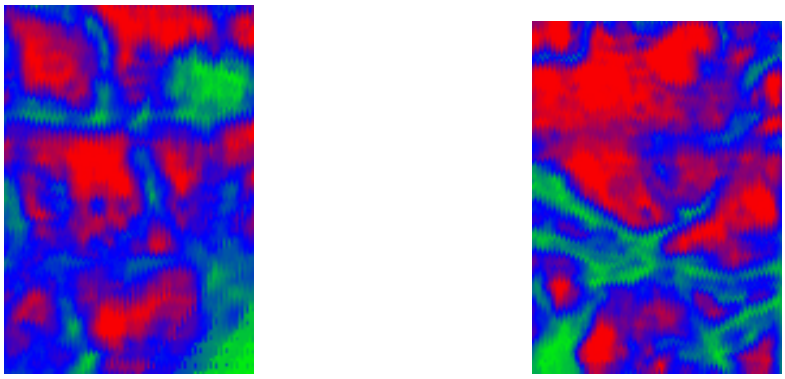

(a) (b)

Figure 4.41 (a) Pre and (b) post impact C-scan image of Group 4 specimen with impact energy of 330J at rib

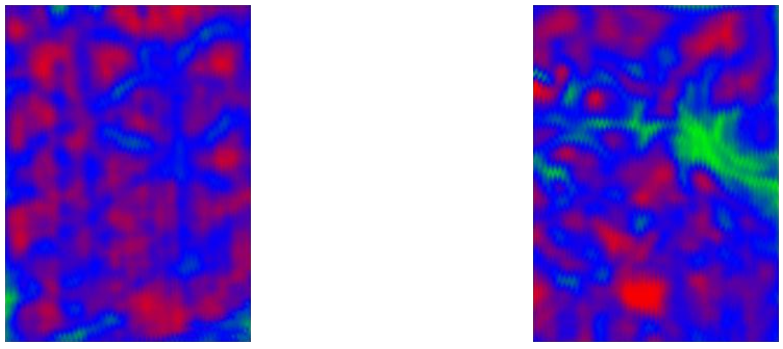

(a) (b)

Figure 4.42 (a) Pre and (b) post impact C-scan image of Group 5 specimen with impact energy of 108J at node

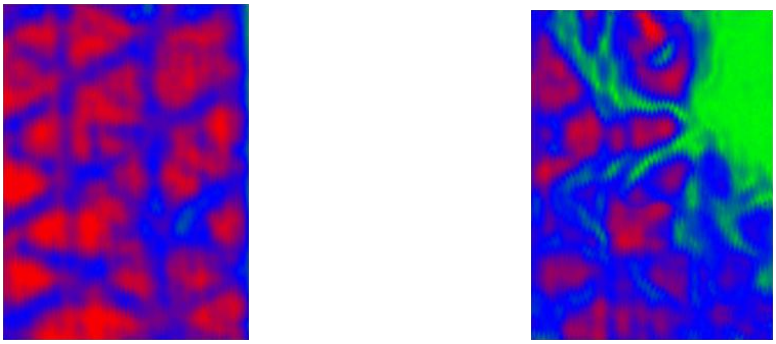

(a) (b)

Figure 4.43 (a) Pre and (b) post impact C-scan image of Group 5 specimen with impact energy of 192J at node

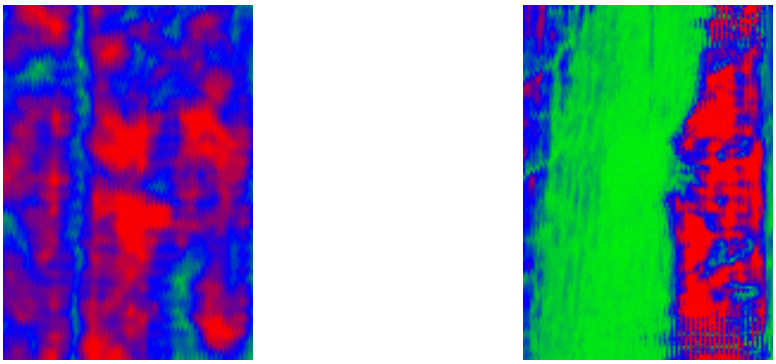

(a) (b)

Figure 4.44 (a) Pre and (b) post impact C-scan image of Group 5 specimen with impact energy of 330J at node

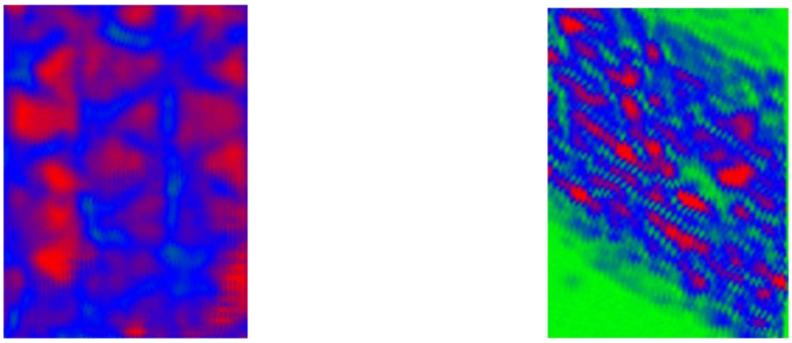

(a) (b)

Figure 4.45 (a) Pre and (b) post impact C-scan image of Group 5 specimen with impact energy of 108J at bay

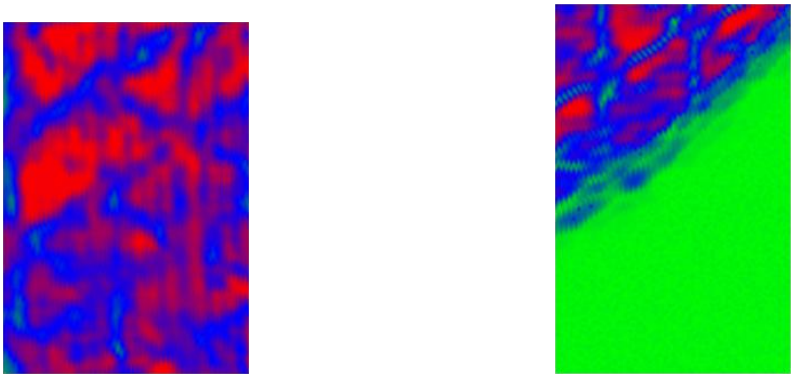

(a) (b)

Figure 4.46 (a) Pre and (b) post impact C-scan image of Group 5 specimen with impact energy of 192J at bay

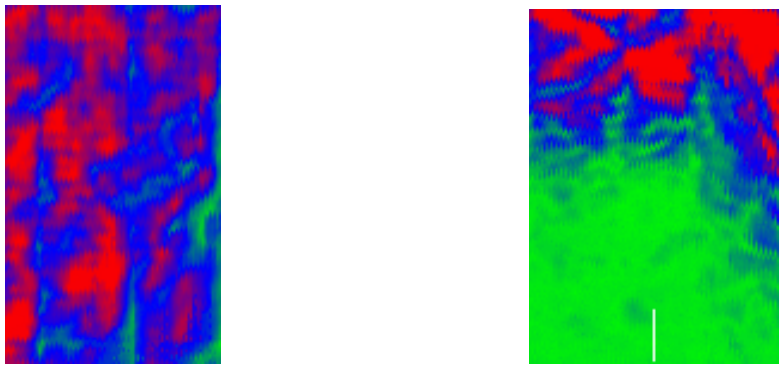

(a) (b)

Figure 4.47 (a) Pre and (b) post impact C-scan image of Group 5 specimen with impact energy of 330J at bay

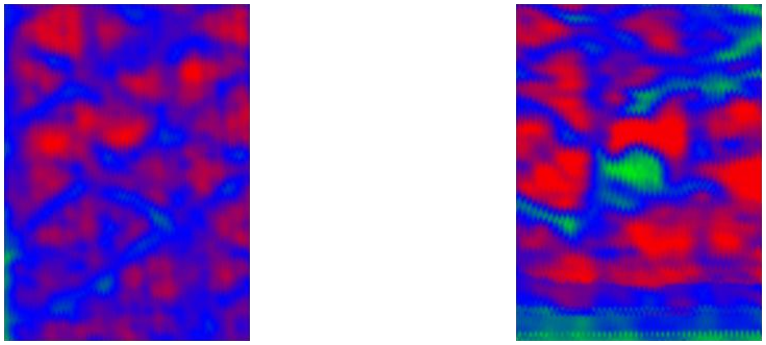

(a) (b)

Figure 4.48 (a) Pre and (b) post impact C-scan image of Group 5 specimen with impact energy of 108J at rib

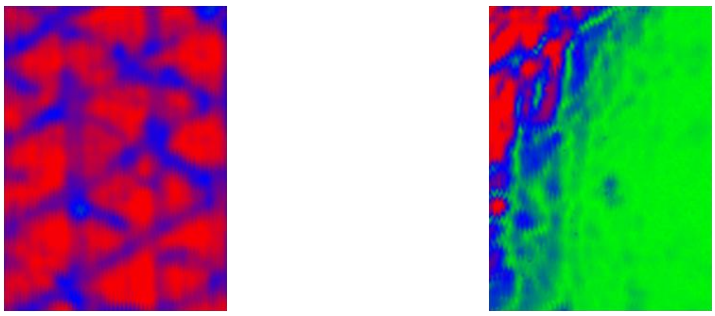

(a) (b)

Figure 4.49 (a) Pre and (b) post impact C-scan image of Group 5 specimen with impact energy of 192J at rib

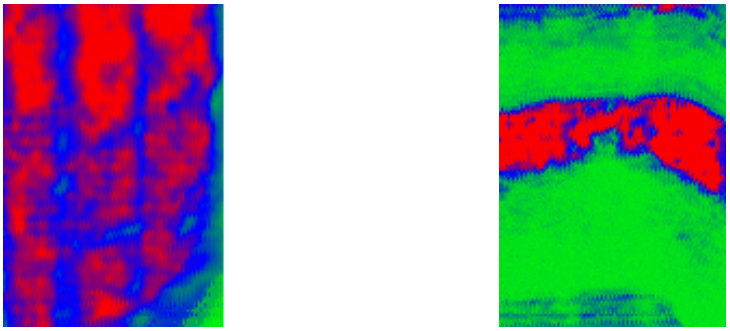

(a) (b)

Figure 4.50 (a) Pre and (b) post impact C-scan image of Group 5 specimen with impact energy of 330J at rib

4.2.3 Compression Testing

Compression Testing is performed on the specimens before and after impact in order to determine the modulus and strength before and after impact. The values of the residual modulus and residual strength for Group 1 to Group 5 are presented in Tables 4.4 - 4.8, respectively. Residual Modulus of the specimens subjected to impact is calculated. Group 5 has the highest modulus for the unimpacted specimens. The modulus of the unimpacted Group 4 sample is lower when compared to other groups of specimens. The reason for this might be that Group 4 specimens have very few closed bays and the percentage area covered by the bay is more when compared with other Groups.

From the results of compression testing it can be observed that the specimens impacted at bay has higher modulus when compared with that of node and rib. The specimens impacted at bay were able to retain most of the strength. The specimens impacted at node have the least modulus. This is because the impact damage in the bay is confined locally by the grid skeleton or the surrounding ribs. Also, the load carrying component is the grid skeleton, not the foam in the bay. Therefore, although the bay suffered from the highest impact damage (the highest propagation energy), its residual strength is still the highest. This provides direct evidence to this idea, i.e., the foam in the bay is secondary in terms of carrying in-plane load; its primary function is to absorb impact energy during impact. If impact is on the ribs, the one damaged rib will affect the load carrying capacity of two neighboring cells. Therefore, even though the damage is still limited to one rib, its effect has been multiplied by the neighboring cells, leading to lower residual strength and stiffness than the impact on bay. If the impact is on the node, due to the intersecting of three ribs instead of two as in the ortho-grid, its effect is at least felt by six ribs and six bays instead of four in ortho-grid. Therefore, the impact on the node is more sensitive than on the rib or on the bay. This may explain the opposite trend in the residual strength as compared to the ortho-grid. Figure 4.51 shows a Group 4 specimen placed in a compression after impact fixture. Tables 4.4 – 4.8 show the modulus and yield stress values of the specimens from Groups1-5. The residual modulus and residual strength values are computed using the stress vs. strain plots obtained from the MTS Test Works software. Group 4 specimens impacted at node have the least values of residual modulus and residual strength when the specimens are subjected to impact energy of 108J and 192J. Group 1 specimens showed least values of residual modulus and residual strength when the specimens are subjected to impact energy of 330J. From the results of residual strength it can be observed that the grid specimens are more stable than the

laminate at higher impact energy of 330J. The probability that a specimen can be impacted at bay, node and rib for a group 2 specimen is 0.61, 0.049 and 0.34 respectively. Similarly for Group 3 the probability that a specimen can be impacted at bay, node and rib are 0.66, 0.04 and 0.30 respectively. For Group 4 specimens, the probability that a specimen can be impacted at bay, node and rib are 0.734, 0.026 and 0.24 respectively. It can be observed that probability of impact at bay region of the specimen is higher when compared to that of node and rib. Also the weakest region which is the node location has very less probability to be impacted when compared to bay and rib.

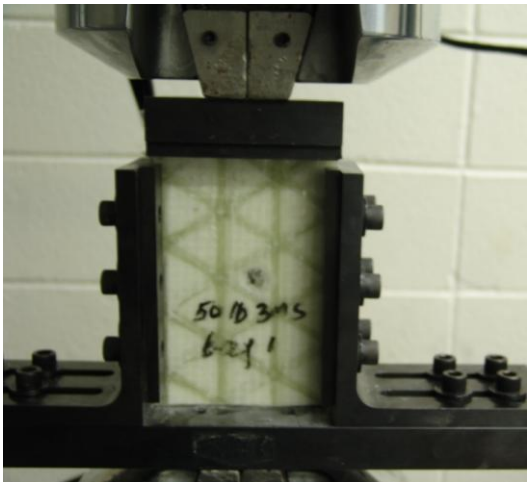

Figure 4.51 Specimen placed in the compression fixture

Table 4.4 Modulus and residual strength values of Group 1 specimens

Mass of hammer (kg)	Velocity (m/s)	Modulus (MPa)	Standard Deviation	Residual Modulus (%)	Residual Strength (MPa)	Standard Deviation	Residual Strength (%)
0	0	2855	266.3	-	34.32	2.58	-
24.09	3	2117	82.1	74.1	22.59	1.49	65.82
	4	1132	49.7	39.6	18.04	1.71	52.56
41.33	4	294	16	10.3	5.87	0.39	17.1

Table 4.5 Modulus and residual strength values of Group 2 specimens

Mass of hammer (kg)	Velocity (m/s)	Impact location	Modulus (MPa)	Standard Deviation	Residual Modulus (%)	Residual Strength (MPa)	Standard Deviation	Residual Strength (%)
0	0	-	2808	277	-	33.31	3.10	-
24.09	3	Bay	2485	140	88.49	27.82	2.05	83.51
		Node	1475	139	52.52	15.04	1.21	45.15
		Rib	1519	139	54.09	18.01	0.97	54.06
24.09	4	Bay	2365	280	84.22	20.78	1.42	62.38
		Node	1187	108	42.27	12.65	1.12	37.97
		Rib	1342	113	47.79	15.32	0.85	45.99
41.33	4	Bay	1560	127	55.55	19.54	1.66	58.46
		Node	479.7	37.69	17.09	8.16	0.48	24.49
		Rib	942.5	38.9	33.35	10.72	1.09	32.18

Table 4.6 Modulus and residual strength values of Group 3 specimens

Weight of hammer (kg)	Velocity (m/s)	Impact location	Modulus (MPa)	Standard Deviation	Residual Modulus (%)	Residual Strength (MPa)	Standard Deviation	Residual Strength (%)
0	0	-	2780	260.0	-	33.49	2.63	-
24.09	3	Bay	1980	98.8	74.3	24.70	1.96	73.75
		Node	1433	86.1	53.8	14.01	1.21	41.83
		Rib	1570	120.1	58.9	19.55	1.64	58.37
24.09	4	Bay	1575	103.5	59.1	18.58	0.86	55.48
		Node	1280	111.5	48.1	11.62	0.45	34.69
		Rib	1358	83.1	51.0	16.52	1.13	49.32
41.33	4	Bay	1429	37.5	53.6	15.53	1.54	46.37
		Node	877	31.5	32.9	9.68	0.37	28.90
		Rib	937	10.8	35.2	12.96	0.77	38.69

Table 4.7 Modulus and residual strength values of Group 4 specimens

Mass of hammer (kg)	Velocity (m/s)	Impact location	Modulus (MPa)	Standard Deviation	Residual Modulus (%)	Residual Strength (MPa)	Standard Deviation	Residual Strength (%)
0	0	-	2474	109.5	-	29.33	2.14	-
24.09	3	Bay	1654	78.6	66.9	22.49	1.94	76.68
		Node	1187	61.6	47.9	10.79	0.71	36.78
		Rib	1194	29.8	48.2	15.22	0.58	51.89
24.09	4	Bay	1611	140.8	65.1	19.32	1.44	65.87
		Node	925	127	37.4	7.90	0.61	26.93
		Rib	1140	86.9	46.2	12.52	1.03	42.68
41.33	4	Bay	1218	108	49.2	14.18	0.88	42.34
		Node	321	18	12.9	5.94	0.31	20.25
		Rib	714	57	28.9	8.78	0.49	29.93

Table 4.8 Modulus and residual strength values of Group 5 specimens

Mass of hammer (kg)	Velocity (m/s)	Impact location	Modulus (MPa)	Standard Deviation	Residual Modulus (%)	Residual Strength (MPa)	Standard Deviation	Residual Strength (%)
0	0	-	3010	225	-	37.67	3.17	
24.09	3	Bay	2541	109	84.4	29.46	2.32	78.21
		Node	1423	150.1	47.3	14.85	1.06	39.42
		Rib	1865	27.7	62.0	18.21	1.42	48.34
24.09	4	Bay	1919	111.4	63.8	23.54	1.97	62.49
		Node	1159	97.4	38.5	11.36	0.78	30.15
		Rib	1732	81.9	56.9	15.97	1.25	42.39
41.33	4	Bay	1542	94.1	51.2	16.19	1.85	42.97
		Node	861	49.6	28.6	9.46	0.63	25.11
		Rib	1125	68.7	37.4	12.78	1.14	33.92

4.2.4 Scanning Electron Microscopy

In order to observe the damage in the iso-grid structures due to impact, Scanning Electron Microscopy (SEM) was performed. Specimens of small cross section were cut from rib and foam region from the region of impact. Samples were cut carefully so that the impact region of the sample was not damaged additionally, and the original damage at micro-length scale can observed. Figure 4.52 shows the crushing of micro balloons of a Group 3 specimen due to impact. Cracks in a matrix due to impact can be observed in Figure 4.53. Debonding of fibers from matrix due to impact can be observed in Figure 4.54 and Figure 4.55 shows the fracture caused in the fiber due to impact.

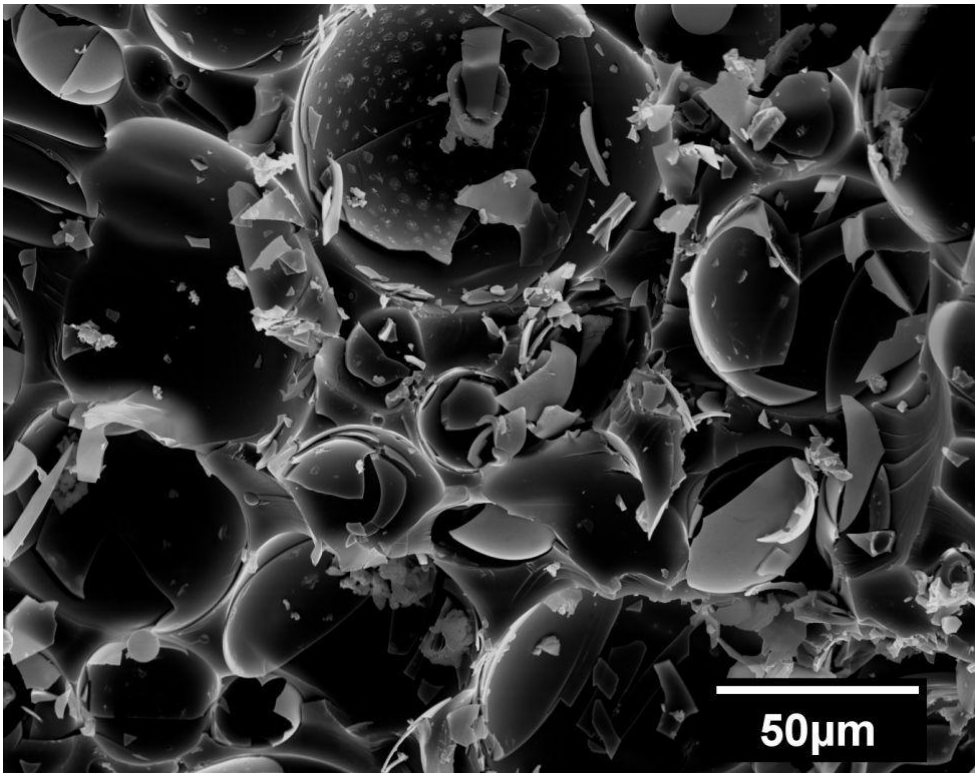

Figure 4.52 Crushing of micro balloons impacted at foam of a Group 3 specimen

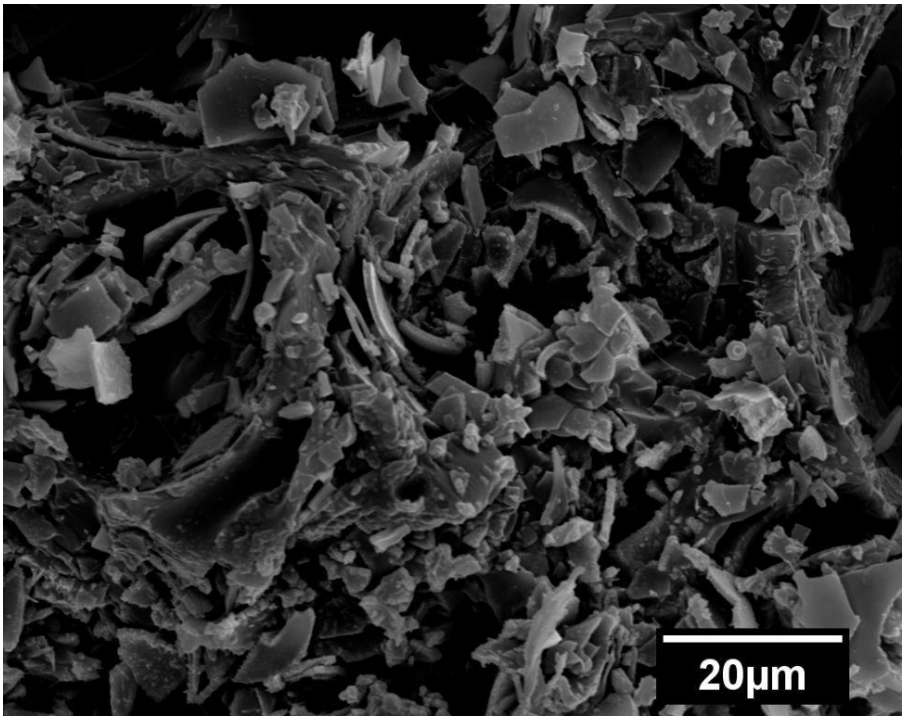

Figure 4.53 Cracking observed in matrix due to the impact

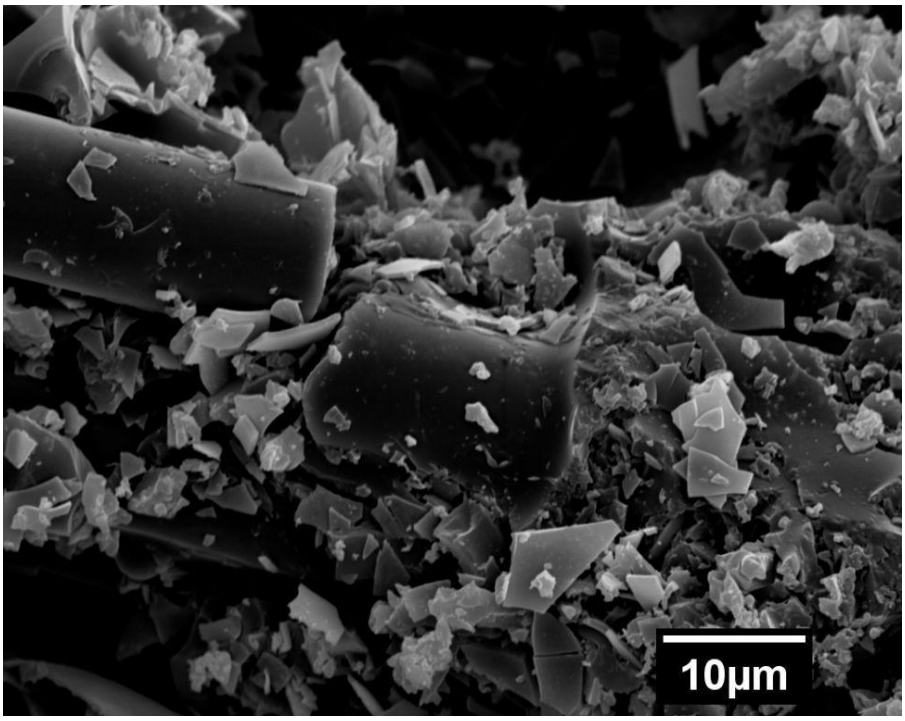

Figure 4.54 Fiber debonding at rib location due to impact

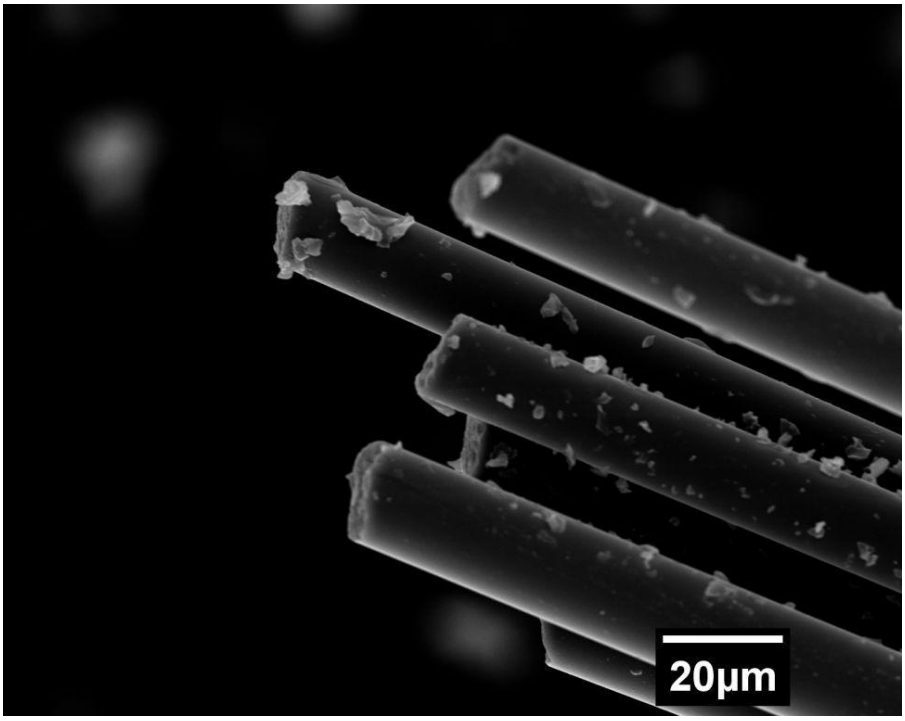

Figure 4.55 Fiber fracture due to impact

CHAPTER 5. FINITE ELEMENT MODELLING OF ISO-GRID STRUCTURES

Finite element analysis of iso-grid structures is performed using ANSYS V11.0. The finite element analysis is performed to validate the experimental results obtained from the iso-grid structures of different bay areas. In order to verify the effect of different parameters on the iso-grid stiffened sandwich structures, parametric study is also performed by varying different parameters like rib thickness, skin thickness and bay area. Modeling and analysis are performed on different models with different bay areas. The different bay areas used in creating the models are 12.7mm×12.7mm, 25.4mm×25.4mm, 50.8mm×50.8mm, 25.4mm×25.4mm with vertical ribs and a laminate. Figure 5.1 shows an unmeshed Group 3 model with skin.

Figure 5.1 Model showing a group 3 specimen with skin

5.1 Modeling Procedure

The dimensions of all the models are 152.4mm×101.6mm×15.24mm and are of the same dimensions as used in the experiments. The key points at the boundary of the iso-grid are created by considering all the end points of the ribs and areas are created using the key points. The areas are extruded to form volumes which give us the grid pattern. All the areas are overlapped in order to obtain separate volumes of nodes, ribs and bay. All the volumes are then glued together. The foam is created in the bays and then skin is placed on top and bottom of the grid skeleton. The element type is defined and the material properties are also defined. The same element type is used for all the entities. The material properties are defined for ribs, nodes and foam. Meshing attributes are defined for nodes, ribs, foam and skin and the properties corresponding to their location are assigned. An element size of 3mm is used to mesh the skin, ribs and foam. For meshing the nodes an element size of 1mm is used. After the attributes are defined, mesh tool is selected, all the element size for each entity is defined and each element is selected separately and meshing is performed on the corresponding entity. Meshing is performed using a solid 45 element which is used for 3-D modeling of solid structures. A solid 45 element has eight nodes which have 3 degrees of freedom in x, y and z directions. The total numbers of elements used for meshing the model are 51112. Figure 5.2, Figure 5.3, Figure 5.4, Figure 5.5 show the foam, ribs, nodes and skin of the model respectively. Once, the model is ready boundary conditions are given and loading is applied along the y-direction on the top surface of the grid. The node region is the intersection of two or more ribs. All the overlapped regions are considered as the node during the modeling. In Figure 5.4 it can be observed that the nodes look like stars. The reason for this is that the ribs interest with each other with an angle other than 90^{o} and usually there are more than six ribs interesting at the same node.

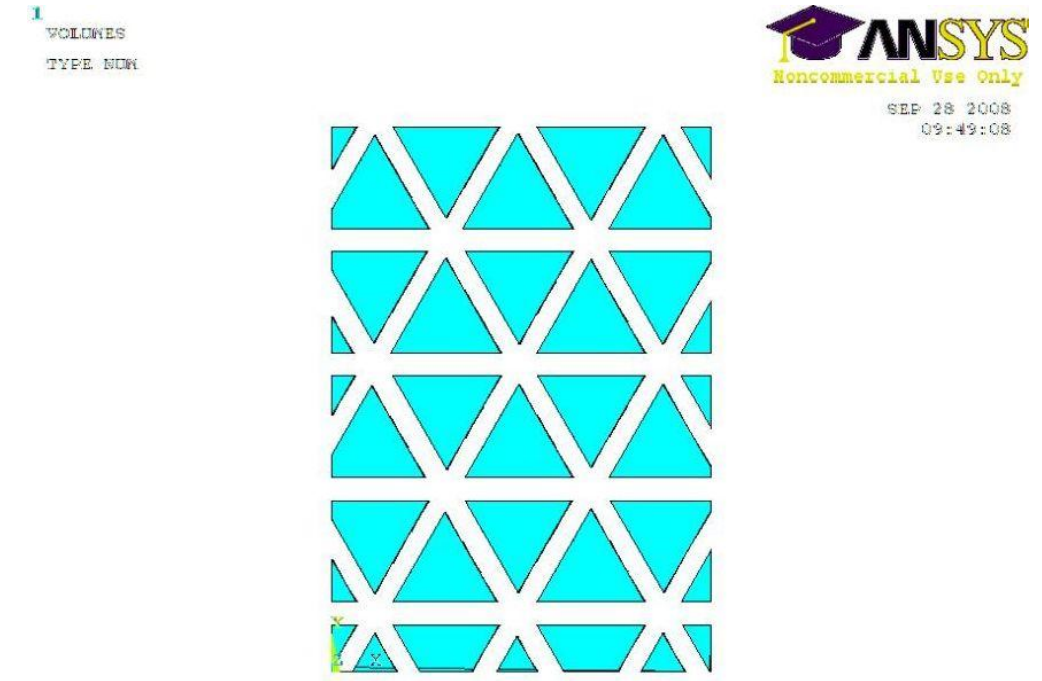

Figure 5.2 Foam from a Group 3 model

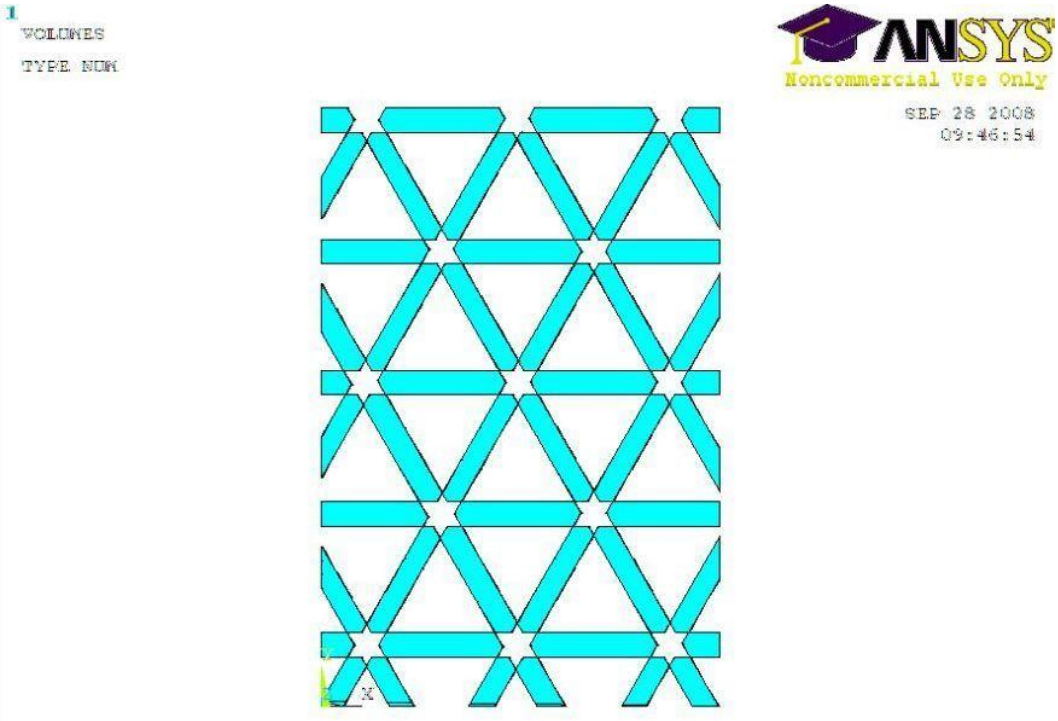

Figure 5.3 Ribs in a Group 3 model

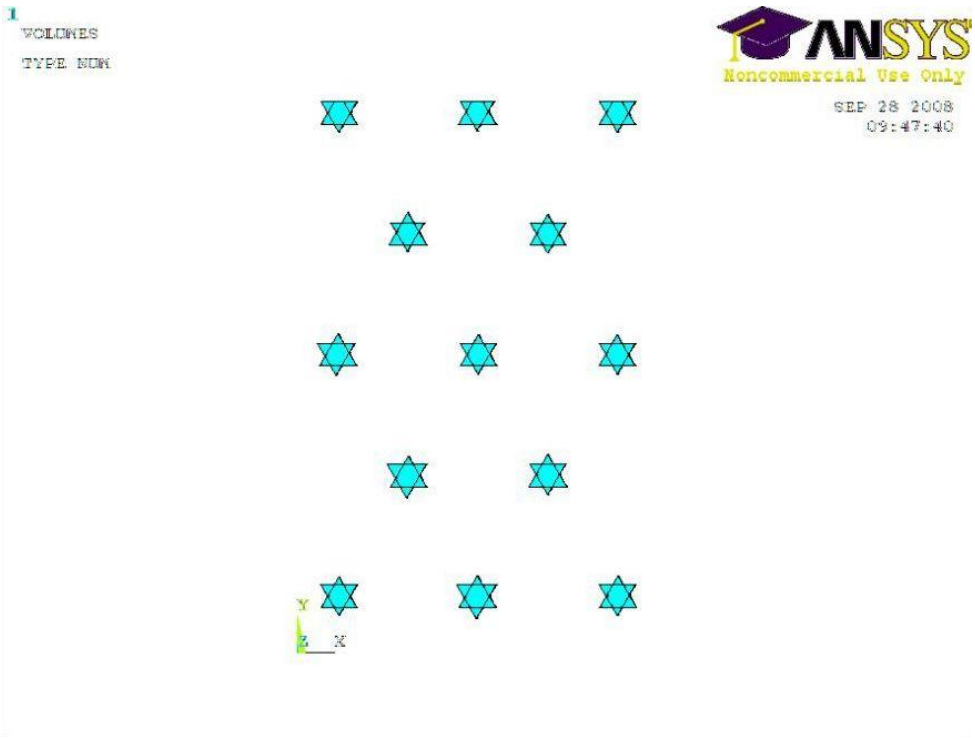

Figure 5.4 Nodes in a Group 3 model

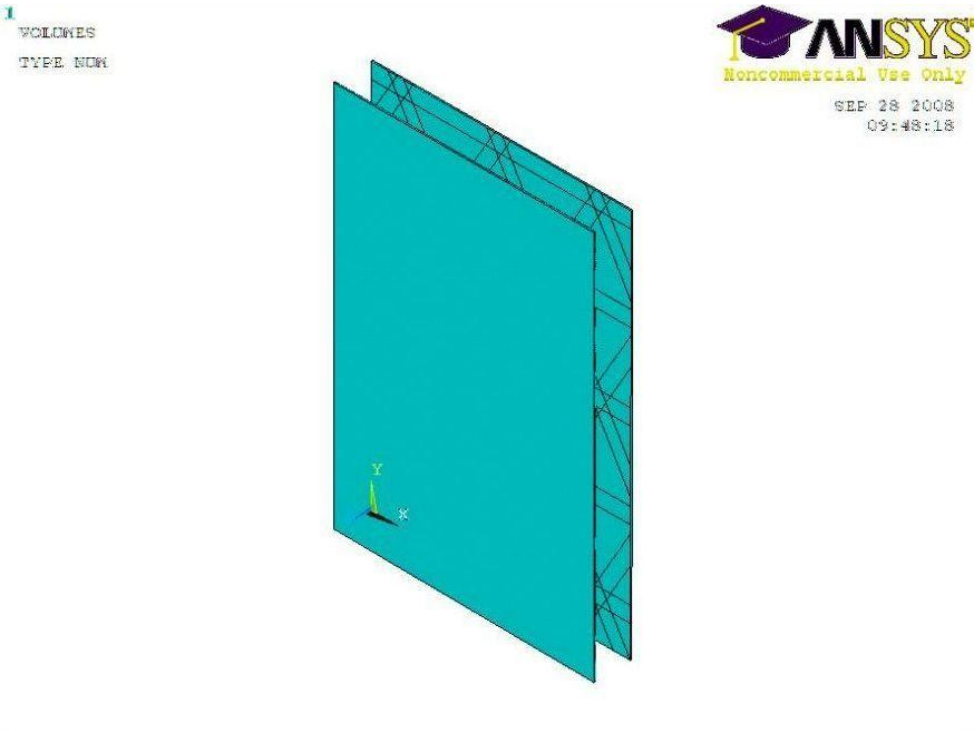

Figure 5.5 Skin from a Group 3 model

5.2 Boundary Conditions and Loading

In order to maintain the same conditions as in the compression testing, the following boundary conditions are used.

1) The bottom face as shown in Figure 4.51 is constrained in the y-direction.
2) The two sides are constrained in both x and z directions
3) Displacement in the y direction was applied on the top surface to simulate the rigid platen used during the loading process in the anti-buckling fixture.

5.3 Convergence Check

In order verify the accuracy of the results from FEM, convergence check is conducted using three different mesh sizes. A fine mesh size of 3mm, medium mesh size of 3.5mm and a coarse mesh size of 4mm were used. A Group 3 specimen is used to perform the analysis. The values of stress are calculated using the loads obtained from the analysis. The results are said to converge if the following criterion is satisfied.

$$|\sigma_F - \sigma_M| \leq |\sigma_M - \sigma_C|$$

The following values are obtained from the FEM when a displacement of 1.95mm is applied in the Y-direction for the three different mesh sizes.

$$\sigma_F = 39.31 \text{ MPa}, \sigma_M = 39.23 \text{MPa}, \sigma_C = 39.13 \text{MPa}$$

$$|\sigma_F - \sigma_M| = 0.08 \text{ MPa and } |\sigma_M - \sigma_C| = 0.12 \text{ MPa}$$

Therefore the condition of convergence has been satisfied and we can say that the results obtained from this analysis are accurate.

5.4 Analysis

Linear static analysis is conducted on Groups 1-5 and the results are compared with the experimental results. A displacement of 1.95mm is applied on all the models and the corresponding modulus values are computed. The value of deflection at yield point for Groups 1-5 is equal to or higher than 1.95mm. Therefore, each Group is considered to be elastic when the displacement is less than 1.95mm. Table 5.1 shows the experimental and FEM modulus values. Figure 5.6 shows the stress vs. strain curve of experimental and FEM values. The values of modulus from the experiment are obtained from the load vs. displacement curve generated by Test Works software during the testing. Displacement is applied on the top surface along the thickness of the structure and solved for the reaction loads on the specimen which are obtained from ANSYS and the value of modulus is calculated from the loads. From Table 5.1 it can be observed that the experimental values of modulus are slightly lower than the values from FEM. The reason for this might that FEM is conducted using linear static analysis whereas during the experiments materials might behave non-linearly and might also have plastic deformation at higher stress. The Y-component of displacement of a Group 3 specimen is as shown in Figure 5.7.

Table 5.1 Experimental and FEM modulus values obtained with a displacement of 1.95mm

Group	Experimental Modulus (MPa)	Modulus from FEM (MPa)
1	2855	3032
2	2808	2966
3	2780	3073
4	2474	2639
5	3009	3231

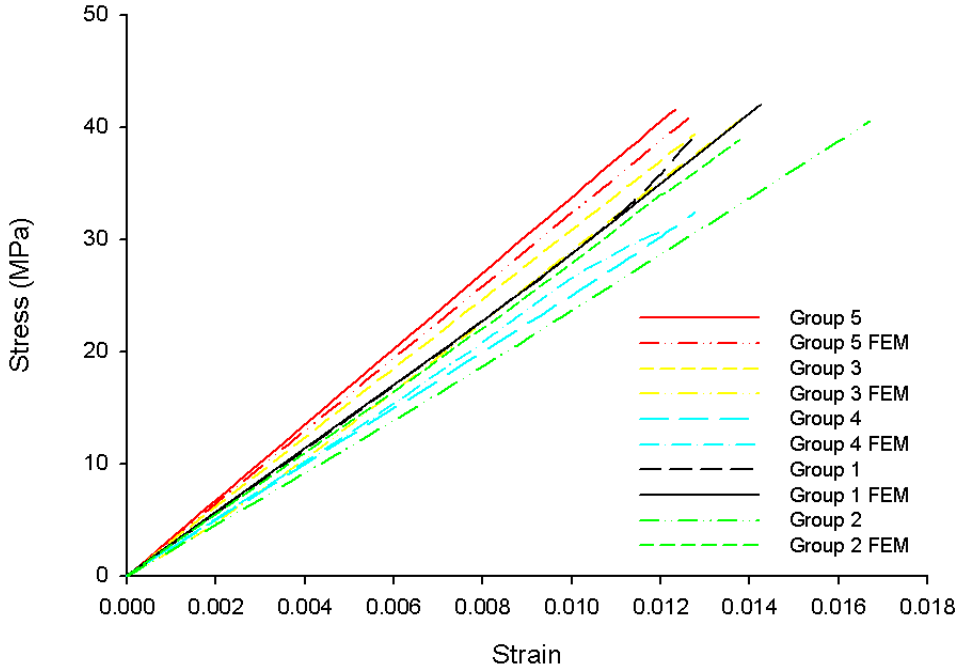

Figure 5.6 Stress vs. strain curve of experimental and FEM values

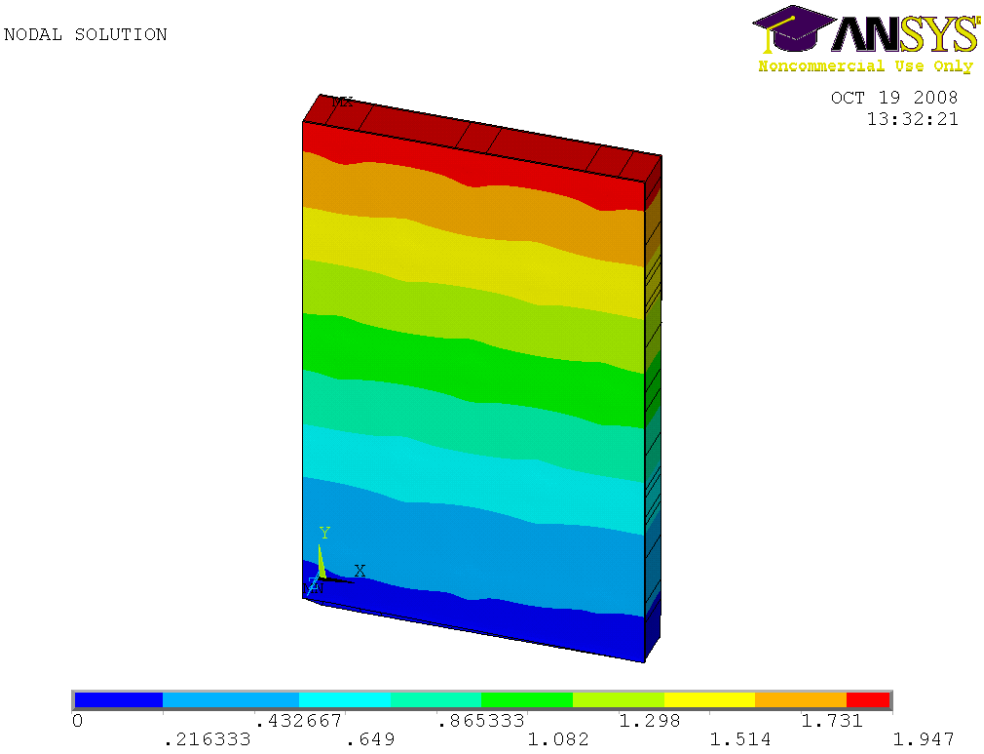

Figure 5.7 Y-component of displacement for a Group 3 model

CHAPTER 6. PARAMETRIC ANALYSIS

After the finite element model showed consistency with the experimental results parametric study is conducted on the iso-grid stiffened sandwich structures. To study the effect of different parameters on the iso-grid stiffened sandwich structures some of the parameters are varied while keeping the fiber volume fraction constant. The same boundary conditions which are used in conducting the static analysis are used in the parametric study. Therefore, the parametric study can answer this question: given the same amount of raw materials (fiber and foam), how does each parameter affect the load carrying capacity of the iso-grid panels? The parameters which are varied to conduct the parametric study are skin thickness, rib thickness and bay area. The variation of modulus values is observed by varying different parameters like skin thickness, rib thickness and bay area. Group 3 specimen which has a 25.4mm×25.4mm bay area is used in the parametric study as a baseline structure.

6.1 Effect of Skin Thickness

The skin thickness is varied keeping the other parameters like rib thickness, bay area and volume fraction of fiber in the ribs constant. A compressive displacement of 1.95mm is applied to the top surface of the model. Skin thickness is varied between 0.6mm to 1.5mm. The volume fraction of fiber in the skin is kept constant in all the cases. Since the volume fraction of fiber in the skin is kept constant, values of modulus of the skin varies for each skin thickness. Table 6.1 shows the material properties used for modeling different skin thickness. A single layer of cross-ply skin is used for modeling the skin of the iso-grid model. For the in-plane loading considered in this study, skin acts as a stiffener for ribs and the foam provides confinement to the grid skeleton. Table 6.2 shows the values of volume fraction of fiber and foam in the skin and also

the load and modulus values obtained from FEM. Figure 6.1 shows the variation of modulus with skin thickness. It can be observed from the plot that as the skin thickness is increased from 0.6mm to 1.0 mm the value of the modulus of the iso-grid structure decreased. The value of modulus increased when the skin thickness is increased from 1mm to 1.5mm. The reason for this might be that though the thickness of the skin was increased the effect of the thickness did not affect the load carrying capacity of the skin till a thickness higher than 1mm but the as the skin thickness increased to 1.5mm the effect of the skin thickness is observed as the modulus of the skin increased. Figure 6.2 shows the effect of variation of skin thickness on the stress vs. strain curve of Group 3 model. Of the three different configurations used, it is observed that a skin thickness of 1mm has the least strength and 0.6mm has highest strength.

Table 6.1 Material properties used in ANSYS for different skin thickness

	0.6mm	1mm	1.5mm
E1	22231.35	13804.81	9591.54
E2	22231.35	13804.81	9591.54
E3	2842.11	1803.55	1524.94
G12	1111.46	704.82	595.82
ν12	0.261	0.269	0.273

Table 6.2 The values of load and modulus with varying skin thickness

Skin thickness (mm)	Load (N)	Modulus (MPa)	Volume fraction of fiber (%)	Volume fraction of foam (%)
0.6	60882	3073	0.61	0.39
1	51431	2596	0.36	0.64
1.5	55552	2804	0.24	0.76

6.2 Effect of Rib Thickness

In this study the thickness of the rib is varied keeping the volume fraction of the fiber constant. The width of the rib is varied from 4mm to 7mm in increments of one. The volume fraction of the fiber constant the values of rib modulus will be changed.

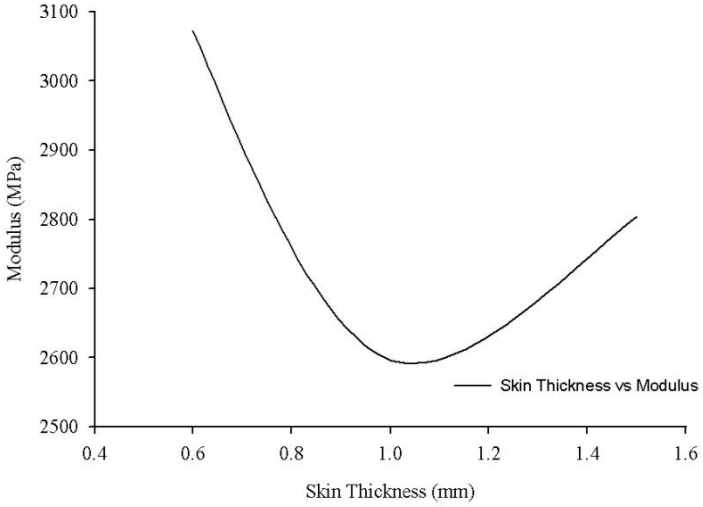

Figure 6.1 Variation of modulus with skin thickness

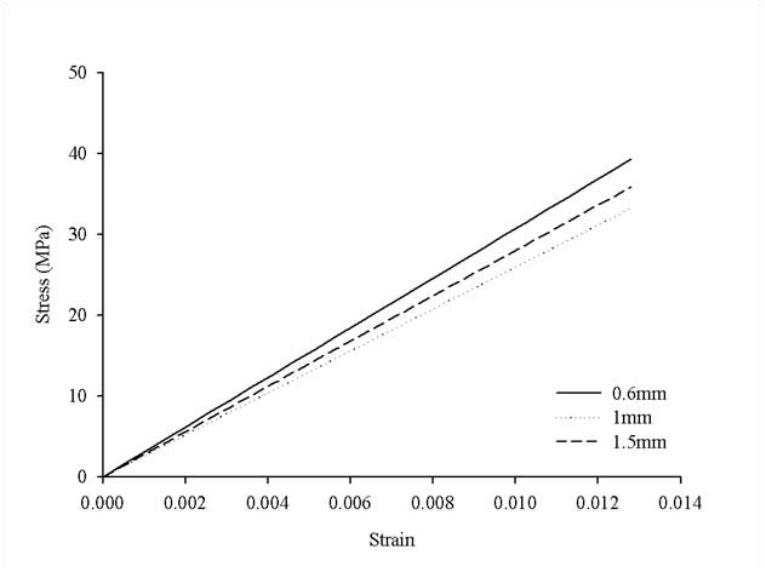

Figure 6.2 Effect of variation of skin thickness on the stress vs. strain curve of Group 3 model

The values of rib modulus are given in Table 6.3. A displacement of 1.95mm is applied on all the models. Figure 6.3 shows the variation of modulus with rib thickness. It can be observed from the figure that has the rib width increases keeping the volume fraction constant, modulus of the specimen decreases. The decrease of the modulus value is not considerable for different cases. Because of the increase in the rib thickness while keeping the volume fraction constant the density of the fiber in the ribs decreases which results in the lower value of modulus as the rib thickness increases. Table 6.4 shows the values of load and modulus obtained from FEM by varying the rib thickness.

Table 6.3 Material properties used in ANSYS for different rib thickness

	4mm	5mm	6mm	7mm
E1	11083.86	9108.05	7830.25	6897.81
E2	1613.21	1498.38	1432.43	1387.86
E3	1613.21	1498.38	1432.43	1387.86
G12	630.35	585.437	559.64	542.21
ν12	0.251	0.253	0.254	0.255

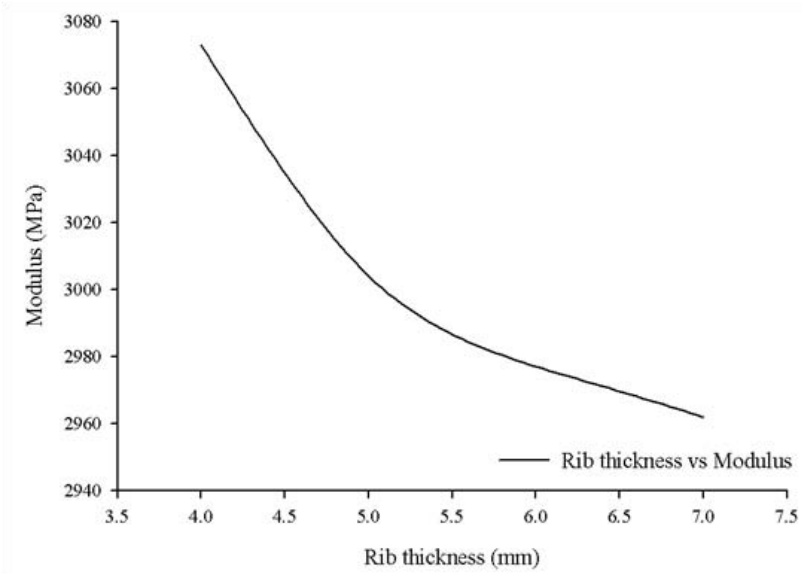

Figure 6.3 Variation of modulus with rib thickness

Table 6.4 The values of load and modulus with varying rib thickness

Rib thickness (mm)	Load (N)	Modulus (MPa)	Volume fraction of fiber (%)	Volume fraction of foam (%)
4	60882	3073	0.287	0.713
5	59507	3004	0.230	0.770
6	58994	2977	0.193	0.807
7	58688	2962	0.166	0.834

6.3 Effect of Bay Area

The variation of modulus by varying the bay areas of the iso-grid is observed. The observation is conducted on laminate which has a bay area of zero, 12.7mm×12.7mm, 25.4mm×25.4mm, 50.8mm×50.8mm, 101.6mm×101.6mm. The material properties used for modeling different bay areas are as shown in Tables 3.6 - 3.10. Figures 6.4 – 6.7 show the grid patterns of various models used. The thickness of the fiber in 25.4mm×25.4mm is slightly higher than that of 12.7mm×12.7mm, therefore the value of rib modulus of the former is slightly higher than the latter which might be one of the factors for the increase in modulus in the former case when compared to the latter. In the case of 50.8mm×50.8mm bay area, even though the value of rib modulus is higher than the case of 25.4mm×25.4mm, in the given dimension of the model for the former there are few number of completed bays which would decrease the number of ribs carrying the load, thus affecting the load carrying capacity. In the case of 101.6mm×101.6mm bay area there is only one complete bay as shown in Figure 6.7, as a result very few ribs are present in the grid structure resulting in further decrease of modulus than compared to other Groups. Figure 6.8 shows the plot for the variation of modulus with the increasing bay area. Figures 6.4 – 6.7 show the grid models for different Groups. From the figures it can be observed that all the grid models have triangles with incomplete boundary for a given dimension of the sample. Group 2, Group 3, Group 4 and a 101.6mm×101.6mm models have only 57%, 34.2%,

45%, and 16.67% of complete boundary. This might be the reason for a lower modulus value for models of some iso-grid stiffened sandwich structures when compared to the laminate.

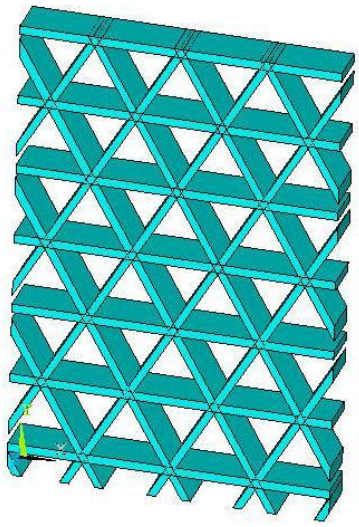

Figure 6.4 Ribs of FEM model used for a 12.7mm×12.7mm bay area

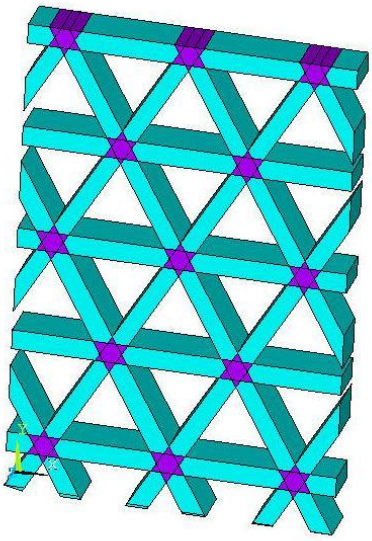

Figure 6.5 Ribs of FEM model used for a 25.4mm×25.4mm bay area

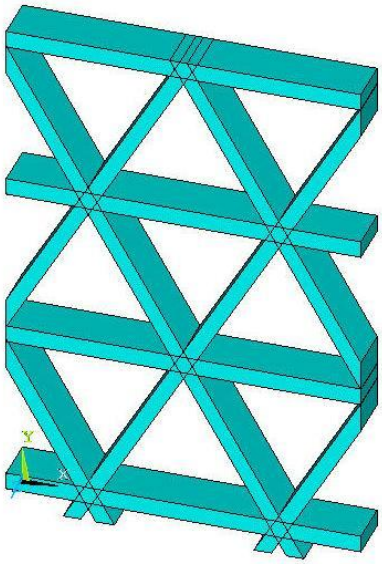

Figure 6.6 Ribs of FEM model used for a 50.8mm×50.8mm bay area

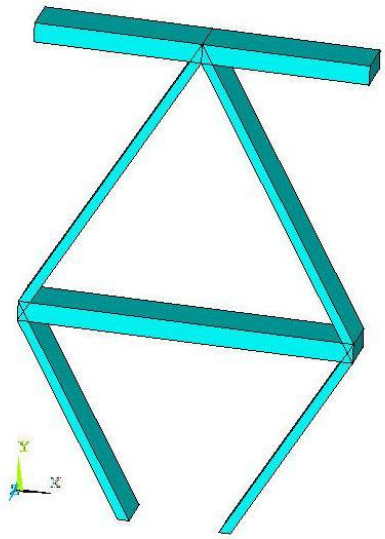

Figure 6.7 Ribs of FEM model used for a 101.6mm×101.6mm bay area

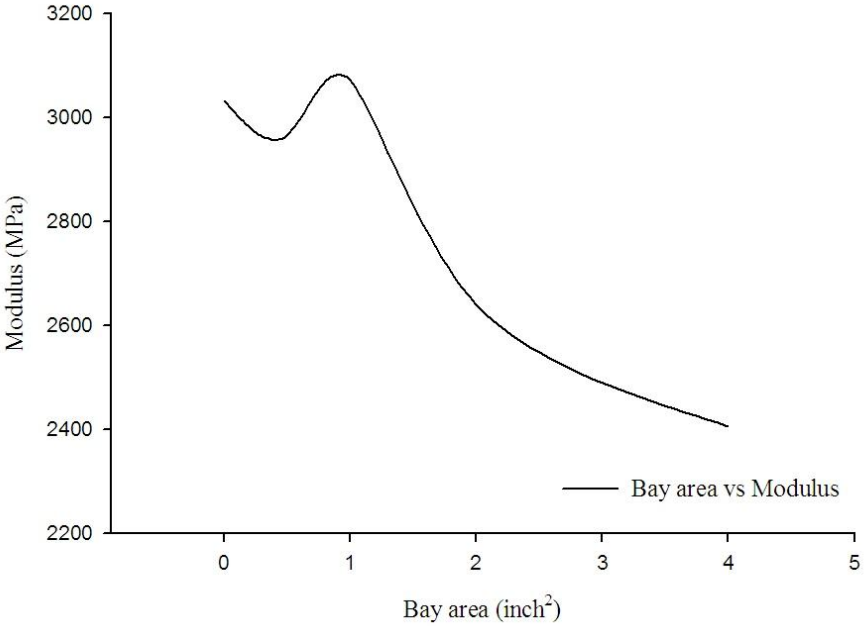

Figure 6.8 Variation of modulus with bay area

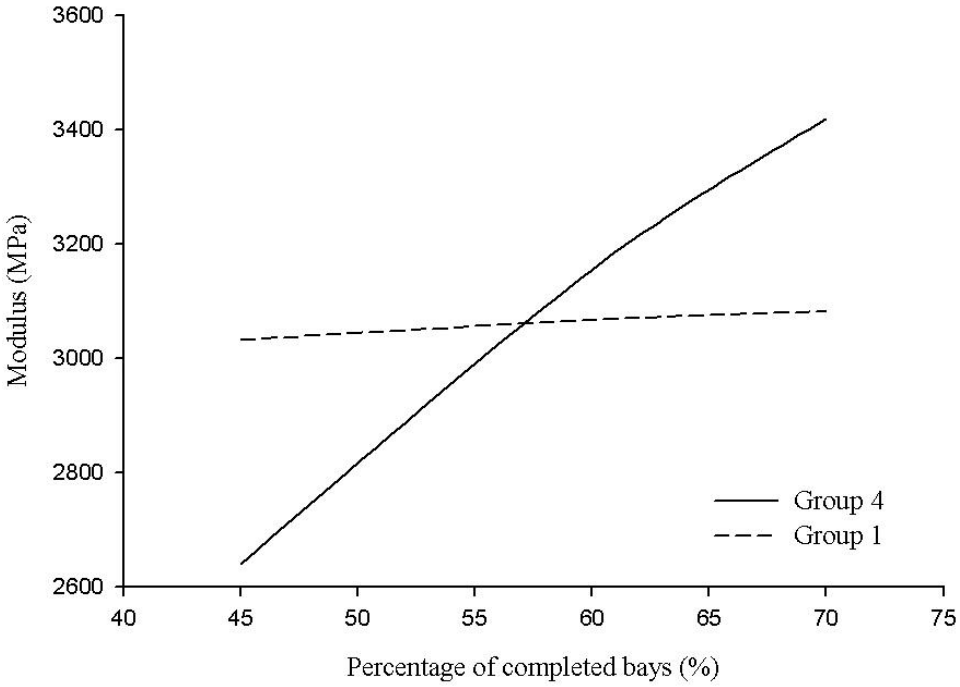

Figure 6.9 Modulus vs. Percentage of completed bays

6.4 Effect of the Percentage of Completed Bays

The effect of the percentage of completed bays on the modulus of the specimens is studied. The percentage of completed bay for a Group 4 specimen of dimension 152.4mm×101.6mm×15.24mm specimen is 45%. In this case, parametric study is conducted for different cases of 60% and 70% completed bays. Laminate with the same dimensions as in the case of Group 4 specimens of 60% and 70% completed bays are modeled and analyzed. The values of modulus of the described models for Group 1 and 4 are compared. The dimension of the model with 60% completed bays is 149.5mm×99.7mm×15.24mm and the dimension of the model with 70% completed bays is 241.3mm×161mm×15.24mm. The variation of the values of modulus with the percentage of completed bays is shown in Figure 6.9 and the values of modulus corresponding dimensions are given in Table 6.5. It can be observed that the values of modulus for Group 4 specimens are increasing with the percentage of completed bays and the increase in the values of modulus for the laminate for the same dimensions of Group 4 specimens is not significant.

Table 6.5 Modulus values of Group 1 and 4 for different dimensions of the specimen

Dimension	Group	Modulus (MPa)
152.4mm×101.6mm×15.24mm	1	3032
	4	2639
149.5mm×99.7mm×15.24mm	1	3067
	4	3155
241.3mm×161mm×15.24mm	1	3082.6
	4	3419

CHAPTER 7. CONCLUSIONS AND FUTURE WORK

7.1 Conclusions

Iso-grid stiffened sandwich structures of different bay areas were fabricated using a pin-guided dry weaving process. In order to reduce imperfections like voids, specimens are placed in vacuum. Post curing of the specimens is performed at a temperature of 100^{o}C for three hours. Low velocity impact test was conducted using two different velocities and two different hammer weights at different locations of node, bay and rib on the iso-grid stiffened sandwich structures. Ultrasonic inspection was conducted on the specimens before and after impact. Compression after impact test was done on the samples to find the residual strength of the grid structure. To determine the micro-length scale damage due to impact, scanning electron microscopy was used.

The analysis of impact results showed that the node has higher values of initiation energy and least propagation energy whereas bay region has higher values of propagation energy and least initiation energy. With the same amount of fiber and foam iso-grid stiffened sandwich structures usually have higher initiation and propagation energy values when compared to the laminate. When subjected to compression after impact the specimens impacted at node showed the least residual strength. The specimens impacted at bay were able to retain most of the strength. This can be attributed to the fact that a unit cell was able to absorb most of the flexural and shear waves generated due to impact. From the residual strength test it was observed that at higher impact energy the percentage of decrease in the residual strength of the laminate is higher when compared to the iso-grid stiffened sandwich structures.

Finite Element Analysis was performed on ANSYS to validate the experimental results. The responses of specimens from all the groups are close to the experimental results. In order to

study the effect of different parameters on the strength of the iso-grid, parametric study was conducted by taking a Group 3 specimen and changing different parameters of skin thickness, rib thickness and bay area. It was observed that with the increase in rib thickness the modulus of the specimen decreases. With the increase in skin thickness, the value of the modulus decreased until a thickness of 1mm and then increased a little till a thickness of 1.5mm. The modulus of the model increased till the bay area of 25.4mm×25.4mm and then decreased as the bay area increases.

Even though the modulus of the laminate for unimpacted specimens is higher than most of the other groups, iso-grid showed higher modulus at higher energies of 330J. Even for smaller impact energies of 108J and 192J, the specimens impacted at bay area which occupies the major percentage of the iso-grid showed higher strength than the laminate. Even in such unfavourable condition iso-grid seemed to perform better in some conditions than the laminate. So, we expect that given a large boundary iso-grid stiffened sandwich structures would perform better than laminates.

7.2 Future Work

A procedure to make the weaving of grid process automated so that all the ribs will have equal tension. Different varieties of foam, grid and skin materials should be used to check for improved properties of iso-grid stiffened sandwich structures. Also, the effect of impact at different locations in the bay, rib and node region should be studied. In order to enhance the bonding between fiber and foam an infusion processes should be developed. Non-linear analysis of iso-grid stiffened sandwich structures should be investigated. Local buckling analysis of the ribs should be conducted on iso-grid stiffened sandwich structures.

REFERENCES

[1] Karlsson K, Astrom T, "Manufacturing and applications of structural sandwich components", Composites Part A: Applied Science and Manufacturing, 1997, Volume 28 (2), 97-111.

[2] Jack RV, "The Behavior of Sandwich Structures of Isotropic and Composite Materials", 1999

[3] Hosur M, Abdullah M, Jeelani S, "Manufacturing and low-velocity impact characterization of foam filled 3-D integrated core sandwich composites with hybrid face sheets", Composite Structures , 2005, Volume 69 (2),167–181.

[4] Hosur M, Abdullah M, Jeelani S, "Manufacturing and low-velocity impact characterization of hollow integrated core sandwich composites with hybrid face sheets", Composite Structures, 2004, Volume 65 (1), 103-115.

[5] Kim CG, Jun E, Impact resistance of composite laminated sandwich plates. Composite Materials, 1992, Volume 26(15), 2247–61.

[6] Herup EJ, Palazotto AN, "Low velocity impact damage initiation in graphite/epoxy/nomex honeycomb-sandwich plates", Composites Science and Technology, 1997, Volume 57 (12), 1581–98.

[7] Nettles AT, Lance DG, Hodge AJ, "An Examination of Impact Damage in Glass/Phenolic and Aluminum Honeycomb core composite panels" , NASA Technical Paper 3042, 1990.

[8] Vaidya UK, Palazotto AN, Gummadi LN, "Low velocity impact and compression after impact response of Z- pin reinforce core sandwich composites", Journal of Engineering Materials and Technology, 2000, Volume 122 (4), 434-442.

[9] McDonnel Douglas Astronautics Company, "Iso-grid Design Handbook", 1973.

[10] Chen H**,** Tsai SW, "Analysis and Optimum Design of Composite Grid Structures", Journal of Composite Materials, 1996, Volume 30 (4), 503-534.

[11] Huybrechts S, Tsai SW, "Analysis and behavior of grid structures", Composites Science and Technology, 1996, Volume 56 (9), 1001-1015.

[12] Roy L, Ares JR, "Impact failure characteristics in sandwich structures. Part I: Basic failure mode selection", International journal of solids and structures, 2002, volume 39 (16), 4215-4235.

[13] Roy L, Ares JR, "Impact failure characteristics in sandwich structures. Part II: Effects of impact speed and interfacial strength", International journal of solids and structures, 2002, volume 39 (16), 4237-4248.

[14] Wu CL, Week CA, Sun CT, " Improving Honeycomb core sandwich structures for impact resistance", Journal of Advanced Materials, 1995, Volume 26(4), 41-47.

[15] Li G, Muthyala V, "Impact characterization of sandwich structures with an integrated orthogrid stiffened syntactic foam core", Composites Science and Technology, 2008, Volume 68 (9), 2078-2084.

[16]] Kim H, Kamis M, "Fracture and impact behaviors of hollow micro-sphere/epoxy composites", Composites Part A: Applied Science and Manufacturing, 2001, Volume32 (9), 1311-1317.

[17] Li G, Nji J, "Development of Rubberized Syntactic Foam," Composite Part A: Applied Science and Manufacturing, 2007, Volume 38 (6), 1483-1492.

[18] Karthikeyan CS, Sankaran S, Kishore, "Elastic behavior of plain and fiber-reinforced syntactic foams under compression", Materials Letters, 2004, Volume 58 (6), 995-999.

[19] Woldesenbet E, Gupta N, Jerro HD, "Effect of Microballoon Radius Ratio on Syntactic Foam Core Sandwich Composites", Journal of Sandwich Structures and Materials, 2005, Volume 7 (2), 95-111.

[20] Gupta N, Karthikeyan CS, Sankaran S, and Kishore, "Correlation of Processing Methodology to the Physical and Mechanical Properties of Syntactic Foams With and Without Fibers", Materials Characterization, 1999, Volume 43 (4), 271-277.

[21] Karthikeyan CS, Sankaran S, Kishore, "Flexural Behavior of Fiber-Reinforced Syntactic Foams", Macromolecular Materials and Engineering, 2005, Volume 290 (1), 60-65.

[22] Hazizan A and Cantwell WJ, "The low velocity impact response of foam core sandwich structures", Composites Part B: Engineering, 2002, Volume 33 (3), 237-239.

[23] Vaidya U, Ulven C, Pillay S and Ricks H. "Impact Damage of Partially Foam-filled Co-injected Honeycomb Core Sandwich Composites", Journal of Composite Materials, 2003, Volume 37 (7), 611-626.

[24] Lim TS, Lee CS, Lee DG, "Failure Modes of Foam Core Sandwich Beams under Static and Impact Loads", Journal of Composite Materials, 2004, Volume 38 (18), 1639-1662.

[25] Sjoblom P, Hartness T, Cordel T, "On Low-Velocity Impact Testing of Composite Materials", 1988, Journal of Composite Materials, 1988, Volume 22 (1), 30-52.

[26] Ishai O, Fliel C, "Damage Tolerance of a Composite Sandwich with Interleaved Foam Core." Journal of Composites Technology and Research, 1992, Volume 14 (3), 155-168.

[27] Belingardi G, Vadori R, "Low velocity impact tests of laminate glass-fiber-epoxy matrix composite material plates", International Journal of Impact Engineering, 2002, Volume 27 (2), 213-229.

[28] Schoeppner G, Abrate S, "Delamination threshold loads for low velocity impact on composite laminates", Composites: Part A, 2000, Volume 31(9), 903-915.

[29] Ray BC, Hasan ST, Clegg DW," Evaluation of Defects in FRP Composites by NDT Techniques", Journal of Reinforced Plastics and composites, 2007, Volume 26 (12), 1187-1192.

[30] Cosenza C Cerniglia D Djordjevic BB, "Non-contact ultrasonic inspection of skin/core bond in honeycomb with Lamb waves", Ultrasonics Symposium Proceedings, IEEE, 2002, Volume 1, 749-752.

[29] Li G, Maricherla D, Singh K, Pang S, John M, "Effect of fiber orientation on the structural behavior of FRP wrapped concrete cylinders", Composite Structures, 2006, Volume 74 (4), 475-483.

[31] Woldesenbet E, Kidane S, Pang S, "Optimization for buckling loads of grid stiffened composite panels", Composite Structures, 2003, Volume 60 (2), 159-169.

[32] Li G, "Experimental Study of Hybrid Composite Cylinders," Composite Structures, 2007, Volume 78 (2), 170-181.

[33] Li G, Velamarthy R, "Fabricating, Testing, and Modeling of Advanced Grid Stiffened Fiber Reinforced Polymer Tube Encased Concrete Cylinders," Journal of Composite Materials, 2008, Volume 42(11), 1103-1124..

[34] Han D, Tsai SW, "Interlocked Composite Grids Design and Manufacturing", Journal of Composite Materials, 2003, Volume 37(4), 287-316.

[36] Steven Huybrechts, Stephen Tsai, "Analysis and Behavior of Grid Structures", Composites Science and Technology, 1996, Volume 56 (9), 1001-1015.

[37] Jadhav P, Mantena R, "Parametric optimization of grid-stiffened composite panels for maximizing their performance under transverse loading", Composite Structures, 2007, Volume 77 (3), 353-363.

[38] Kidane S, Li G, Helms J, Pang S, Woldesenbet E, "Buckling load analysis of grid stiffened composite cylinders", Composites: Part B, 2003, Volume 34 (1), 1-9.

[39] Gan C, Gibson RF, Newaz GM, "Analytical/Experimental investigation of energy absorption in grid-stiffened composite structures under transverse loading", Experimental Mechanics, 2004, Volume 44 (2), 185-194.

[40] Chen H, Tsai SW, “Analysis and Optimum Design of Composite Grid Structures”, Journal of Composite Materials, 1996, Volume 30 (4), 503-534.

[41] Li G and Cheng JQ, “A Generalized Analytical Modeling of Grid Stiffened Composite Structures,” Journal of Composite Materials, 2007, Volume 41(24), 2939-2969.

VITA

Venkata Sandeep Chakka completed his schooling in April 2000, at Andhra Pradesh Residential Junior College, Nagarjuna Sagar, Andhra Pradesh, India. He received the degree of Bachelor of Engineering in mechanical engineering from Andhra University, Vishakhapatnam, Andhra Pradesh, India, in 2005. He then joined the graduate program at Louisiana State University, Baton Rouge, Louisiana, in January 2006. He will be graduating in December 2008 with the degree of Master of Science in Mechanical Engineering.

.